AD-771 304

THEORETICAL AND EXPERIMENTAL INVESTIGATIONS OF VORTEX LIFT CONTROL BY SPANWISE BLOWING. VOLUME II. THREE-DIMENSIONAL THEORY FOR VORTEX-LIFT AUGMENTATION

Jerome G. Theisen, et al

Lockheed-Georgia Company

Prepared for:

Office of Naval Research

15 September 1973

DISTRIBUTED BY:

NTIS

National Technical Information Service
U. S. DEPARTMENT OF COMMERCE
5285 Port Royal Road, Springfield Va. 22151

Unclassified

Security Classification

AD 771304

DOCUMENT CONTROL DATA - R & D

(Security classification of title, body of abstract and indexing annotation must be entered when the overall report is classified)

1 ORIGINATING ACTIVITY *(Corporate author)* Lockheed-Georgia Company Flight Sciences Division Marietta, Georgia 30063	2a. REPORT SECURITY CLASSIFICATION Unclassified 2b. GROUP N/A

3 REPORT TITLE

THEORETICAL AND EXPERIMENTAL INVESTIGATIONS OF VORTEX LIFT CONTROL BY SPANWISE BLOWING: VOLUME II, THREE-DIMENSIONAL THEORY FOR VORTEX-LIFT AUGMENTATION

4 DESCRIPTIVE NOTES *(Type of report and inclusive dates)*

Final Technical Report (15 April 1972 to 15 Sept. 1973) (Vol. II of II)

5. AUTHOR(S) *(First name, middle initial, last name)*

Jerome G. Theisen, Roy M. Scruggs, and Charles J. Dixon

6. REPORT DATE	7a. TOTAL NO. OF PAGES	7b NO. OF REFS
15 September 1973	108	43

8a. CONTRACT OR GRANT NO.	9a. ORIGINATOR'S REPORT NUMBER(S)
N00014-72-C-0237	
b. PROJECT NO.	LG73ER-0169
c.	9b. OTHER REPORT NO(S) *(Any other numbers that may be assigned this report)*
d.	

10 DISTRIBUTION STATEMENT

Approved for public release; distribution unlimited

11 SUPPLEMENTARY NOTES	12. SPONSORING MILITARY ACTIVITY
	Aeronautics, Code 461 Office of Naval Research Arlington, Virginia 22217

13 ABSTRACT

A theoretical description is presented on the experimentally observed phenomenon of wing leading-edge vortex lift control by spanwise mass injection. The vortex and jet initial source/sink strengths and locations are established by a conformal mapping solution, and used as starting conditions for an iterative vortex-lattice simulation. The spanwise jet is shown to augment the stability of a vortex which forms at high angles-of-attack in the leading-edge region where wings of moderate-to-high aspect ratio otherwise exhibit fully turbulent separation. Definitive results are obtained on wing lift and corresponding pressure distributions for comparison with the test data presented in Volume I. Certain scale or Reynolds Number effects are formulated, particularly concerning the prediction of flow stability such as vortex burst over the wing or in the near wake. The preliminary results indicate that, possibly, such instabilities are less likely to occur for vortex lift control in full-scale flight. In other respects the differences between model and large scale theoretical predictions are found to be negligible, as is generally confirmed by the high Reynolds Number tests (Volume I).

Reproduced by
NATIONAL TECHNICAL
INFORMATION SERVICE
U S Department of Commerce
Springfield VA 22151

1a

DD FORM 1 NOV 65 1473

Security Classification

108

14. KEY WORDS	LINK A		LINK B		LINK C	
	ROLE	WT	ROLE	WT	ROLE	WT
Aerodynamic Theory						
Aerodynamic testing						
Lift Augmentation						
Control						
Vortex						
Vortex Control						
Vortex Burst						
Turbulent Wake						
Stall						
Smoke Tunnel						
Jets						
Viscous Flow						
Viscous Mixing						
Wind Tunnel Tests						
Laser Doppler Velocimeter						
Powered Lift						
Pressure Distributions						
Entrainment						

16

UNCLASSIFIED

THEORETICAL AND EXPERIMENTAL INVESTIGATIONS OF VORTEX LIFT CONTROL BY SPANWISE BLOWING

VOLUME II

THREE-DIMENSIONAL THEORY FOR VORTEX-LIFT AUGMENTATION

Sept. 15, 1973

by
J. G. Theisen
R. M. Scruggs
C. J. Dixon

Final Report
(15 April 1972 to 15 Sept. 1973)

Prepared under Contract No. N00014-72-C-0237,
Contract Authority NR215-201/1-12-72(461)
for the
Aeronautics, Code 461
Office of Naval Research
Arlington, Virginia 22217

APPROVED: _____

B. H. Little, Jr. Manager
Advanced Flight Sciences Department
LOCKHEED-GEORGIA COMPANY

Reproduction in whole or in part is permitted for any purpose of the United States Government.
Approved for public release; distribution unlimited.

FOREWORD

This research on a unique lift-augmentation concept was performed under Contract No. N00014-72-C-0237 for the Office of Naval Research. Mr. T. L. Wilson was Technical Contract Monitor for Aeronautics, Code 461. The results are reported in the following volumes.

VOLUME I - EXPERIMENTAL RESEARCH

VOLUME II - THREE-DIMENSIONAL THEORY FOR VORTEX-LIFT AUGMENTATION

SUMMARY

An attempt is made in this volume to develop and demonstrate an analytical procedure by which the phenomena of vortex-lift control, using spanwise blowing or mass/momentum addition, can be predicted to a useful degree of accuracy. The approach is predicated on the assumption that the simplest conceptual and heuristic reasoning is to be used where alternatives of more complexity may possess equal or greater plausibility. Within this context a measure of success was achieved in terms of understanding the physical, viscid and inviscid, mechanisms of coaxial jet-and-vortex augmentation and entrainment as the pair are swept outboard and aft over a lifting surface. As anticipated, limitations in the theory became apparent in early stages; but even these results are useful in pointing out the requirements for future research, as well as suggesting even broader vortex theory applications such as possible techniques for controlling or modifying the growth and dissipation of potentially hazardous wing tip vortices.

The theoretical analysis applies two-dimensional, potential flow solutions using conformal mapping to obtain vortex-sink strengths as starting conditions for a three-dimensional vortex lattice simulation. This latter computer program is modified to account for source/sink and viscous vortex interactions with a crossflowing jet. Nearly optimum conditions for vortex-lift augmentation are selected for emphasis in the simulation. Thus, an under-expanded (supersonic) jet is assumed to issue, over a wing at stall attitudes, from a nozzle pointed in an approximate spanwise direction at a chordwise position known to allow a sizeable Helmholtz flow to normally persist due to leading edge separation. The boundary conditions result in a

vortex forming above and aft of the leading edge, as discussed in the experimental work (Volume I); and the three-dimensional solution provides vorticity augmentation through a Stokes' integration of the jet-boundary layer (wall-jet) shear profiles. Empirical hypotheses, such as the Polhamus' leading edge suction analogy, are introduced to justify a rapidly converging iterative procedure which yields numerical solutions.

Definitive results are obtained on wing lift and corresponding pressure distributions for comparison with the test data presented in Volume I. Certain scale or Reynolds Number effects are formulated, particularly concerning the prediction of flow stability such as vortex burst over the wing or in the near wake. The preliminary results indicate that, possibly, such instabilities are less likely to occur for vortex lift control in full-scale flight. In other respects the differences between model and large scale theoretical predictions are found to be negligible, as is generally confirmed by the high Reynolds Number tests (Volume I).

VOLUME II

CONTENTS

LIST OF FIGURES

NOMENCLATURE

a	Jet "set-back" factor
$A_{0,1,2}$	Empirical coefficients (see Appendix A)
b	Wing Span
B	Empirical coefficient (see Appendix A)
c	Local wing chord length
$\bar{c}$	Average wing chord length
C_f	Surface friction coefficient
C_ℓ	Section lift coefficient (2-D)
C_L	Lift coefficient
C_{L_T}	Total aircraft lift coefficient
C_μ	Jet momentum coefficient
C_p	Differential pressure coefficient
C_w	Factor to account for extreme velocity differentials between the upper and lower wing surface represented by a vortex lattice
d_c	Nozzle true diameter
D	Jet decay coefficient (see Appendix A)
D_o	Nozzle effective diameter
e_o	Effective wall-jet surface induction ratio (=.08)
H	Ratio of Helmholtz to potential flow lift for a stalled lifting element
J	Momentum flux
k_{c_1}	Factor in loads estimates to account for extreme velocity gradients in the upper surface viscous (wall-jet) layer
K_a	Two-dimensional airfoil circulatory strength
K_v	Two-dimensional vortex strength

$\bar{K}_n$	Net augmented and dissipated circulation of primary vortex element, n
ΔL	Cross-stream projected length of a given bound vortex element, as per subscripts
m_J	Jet effective source strength (2-D)
m_v	Vortex source/sink strength (2-D)
P	Transformed stream function for a viscous vortex (Appendix B)
P_E	Jet exit pressure
q	Dynamic pressure; or turbulence velocity (Appendix A)
$\dot{Q}$	Volumetric mass flux
r_1	Initial estimate of radius for leading-edge vortex based on the half-jet displacement thickness
r_{c_i}	Radius of the hard-core in the viscous vortex (see Appendix A)
R	Jet cross-flow velocity ratio (see Appendix A)
R_N	Radial-inflow Reynolds Number (see Appendix A)
R_o	Rossby number (see Appendix A)
R_v	$= \Gamma_v/\nu$ Vortex Reynolds Number (see Appendix A)
$\bar{R}$	Resultant distance
S	Area of wing, or wing sub-element as per subscripts; or Strouhal Number
t	Time; or radial stretching-transform variable (Appendix B)
u,U	Velocity in the x direction (unless otherwise indicated)
U_J	Initial jet velocity
U_v	Jet axial velocity component at the vortex location
U_{V-L}	Velocities which lie in vertical streamwise planes and are induced at load points, by the basic vortex-lattice system in the wing

Greek Symbols

α	Angle of attack
β	(See Appendix A)
γ	Jet spread half-angle (Appendix A)
γ_o	Vortex axial growth proportionality
Γ	Circulation
δ	Width of annular turbulent mixing region just beyond the vortex "hard-core" radius, r_i
δ_J	Effective depth of the spanwise jet beneath the primary vortex above the level Δy_m
Δ	Denotes "Incremental" as a prefix
ζ	Transform variable to map z into the circle-plane
ζ_J	Jet position in the ζ-plane
ζ_V	Vortex position in the ζ-plane
ε	A small parameter (Appendix B)
η	$x/(b/2)$, ratio of span station to wing semi-span
θ	Phase angle
θ	Turning angle of jet or vortex centerline as indicated relative to the cross-stream direction, as per subscript
θ_o	Initial jet angle relative to leading edge sweep at wing root
κ	Turbulence proportionality
λ	Taper ratio of wing (except in Appendix A)
Λ	Wing sweep angle
Λ_i (t)	Empirical viscous aging/scale parameter (Appendix A)

ν	Kinematic viscosity
ν_T	Turbulent eddy viscosity
ρ	Fluid mass density
τ	Normalizing time in vortex aging process (Appendix A)
Ω	Spatial frequency (wave number)

Subscripts

am	Denotes ambient fluid conditions
c	Denotes corrected
e	Denotes effective; or nozzle exit conditions as indicated
E	Denotes jet exit fluid conditions
i	Index for spanwise wing station; i = 0 at fuselage sidewall
j	Index for chordwise panel location; j = 1 at wing leading edge panel
J	Designates the jet aparameters or position
ℓ	Denotes section lift (2-D)
L	Denotes total lift
m	Denotes maximum (or wing tip location, as in x_m)
n	Designates the primary vortex element, beginning with n = 1 as the first bound link of the most forward feeding sheet element emanating from the vertical plane of symmetry (fuselage sidewall or centerline)
o	Denotes origin or initial conditions at the jet orifice (nozzle exit)
s	Denotes conditions at end of under-expanded jet region
v	Designates vortex parameters or position
∞	Denotes conditions at infinity

Superscripts, Prefixes, Postscripts

$\bar{}$	Designates a vector quantity (or, an average as in $\bar{v}$)
$\lvert\ \rvert$	Designates absolute value when used as brackets
$\mathcal{O}$	Designates "order of"

1. INTRODUCTORY DISCUSSION

The search for a greater understanding of vortex flows very likely provides one of the most persistent historical goals of fluid mechanics research. The elusive character of vortices, forming and dispersing in sometimes perturbing and often beneficial conditions, is largely dependent upon the stabilizing or destabilizing characteristics of the local flow environment. Basic analytical and experimental research on the mechanisms of vortex flows in bluff body wakes, as described in Reference 1, have resulted in specific means for controlling vortex growth and stability. It is demonstrated therein that the Strouhal frequency in the Von Karman street can be predicted theoretically if, and only if, the three-dimensional viscous Navier-Stokes equations are utilized so that axial vortex flow can be considered. Various means were used in tests (Ref. 1) for modifying the axial mass-flow and vorticity propagation characteristics for vortices forming in near-wake or separated flow regions. Such modifications resulted in elimination of the periodic vortex shedding and restoration of the Foppl vortex pair behind bluff bodies at supercritical Reynolds numbers. Further experiments at that time, reported in References 1 through 5 demonstrated that either suction or blowing parallel to the axis of vortices in cavities, or separated flow regions, could stabilize and "lock" an augmented vortex in position so as to produce direct lift increments. Subsequently, many practical applications have been found and published (Refs. 2, 6-8) concerning both lift and drag as well as stability and control implications.

The present research program extends the earlier research by showing more generalized dependence of the flow control mechanisms upon the Rossby

number (ratio of linear-to-angular momentum) and Radial Inflow Reynolds Number previously discussed in Reference 1. For example, the vortex growth, persistence and stability are of obvious importance to the spanwise blowing, vortex momentum exchange phenomenon. Thus, stability criteria and effectiveness parameters are developed which allow preliminary estimates to be calculated for vortex-lift augmentation applied to more general aircraft configurations. However, future research is required for complete resolution of this problem for final design purposes.

2. TWO-DIMENSIONAL POTENTIAL FLOW ANALYSIS

2.1 BASIS FOR THE MATHEMATICAL MODEL

2.1.1 Experimental Observations

The extensive smoke flow visualization experiments on spanwise blowing have been studied for a wide range of flow conditions. A typical flow pattern is shown in Figure 2 of Volume I. This photograph shows the flow structure in a chordwise vertical plane near the wing root with a jet blowing into the region which would be fully separated at this incidence if no blowing were present. A distinctly discrete vortex is seen downstream of the leading edge separation point but forward of the lateral jet flow. Fluid is observed to spiral in toward the vortex center, suggesting the presence of a sink as viewed in two dimensions. Whatever the complex three-dimensional interaction may be between the jet and the stalled flow field, it seems apparent that the jet causes a vortex to appear and to maintain its existence by inducing an axial flow in the vortex. The apparent sink strength is sufficient to duct fluid mass out the wing span at the same rate at which it is entrained from the leading edge and freestream. The flow downstream of the jet centerline is steady and appears to reattach somewhere along the chord aft of the centerline. For some conditions there are multiple stagnation points along the upper surface of the chord. In every case the flow near the trailing edge is well behaved so that the Kutta-condition may be applied as a necessary condition in the potential flow model. However, these observations of flow pattern apply primarily for angles of attack above the stall angle of the airfoil section being considered. Based on the preceding visual evidence, a mathematical model is formulated as described below.

2.1.2 Mathematical Formulation

Since the leading edge detachment is present in practical cases, a flat plate approximation of the airfoil is considered to be reasonable. This leads to a simpler mathematical representation in the complex plane while retaining the essential vortex lift augmentation effects demonstrated for the wing under test. The other elements of the flow are a vortex, a source/sink at the center of the vortex, and a source to represent the jet. The vortex feeding sheet from the leading edge is not represented in the present model; this leads to a more tractable mathematical solution and is considered to be justified in a first attempt to assess the effects of the more notable flow mechanisms. Also, the representation of the jet in two dimensions as a source requires careful physical interpretation and this subject will be deferred for later discussion.

Conformal mapping techniques are convenient for representing the two-dimensional flow field. The airfoil is taken along the real axis in the Z-plane between (-2, +2) as shown in Figure 1. The jet position, Z_J, and its source strength, m_J, are assumed to be known. To represent typical chordwise sections, this implies a priori knowledge of crossflowing - jet phenomena as discussed in the section on three-dimensional methods. The vortex center is located at Z_V, and it has a circulation strength, K_V; a source/sink, m_V, is also located at Z_V (whether a source or a sink is present will be determined by the sign in the solution). The freestream is set at angle α, as shown in the figure, and it has a velocity magnitude, V_∞. Finally, there is airfoil bound circulation of strength K_a.* The Z-plane is mapped into the circle plane or ζ-plane by,

---

*For convenience a factor 2π is included in the m's and K's, thus the source/sink strength in vol./sec./ft. is $2\pi m$ and the circulation in ft.^{2}/sec. is $2\pi K$.

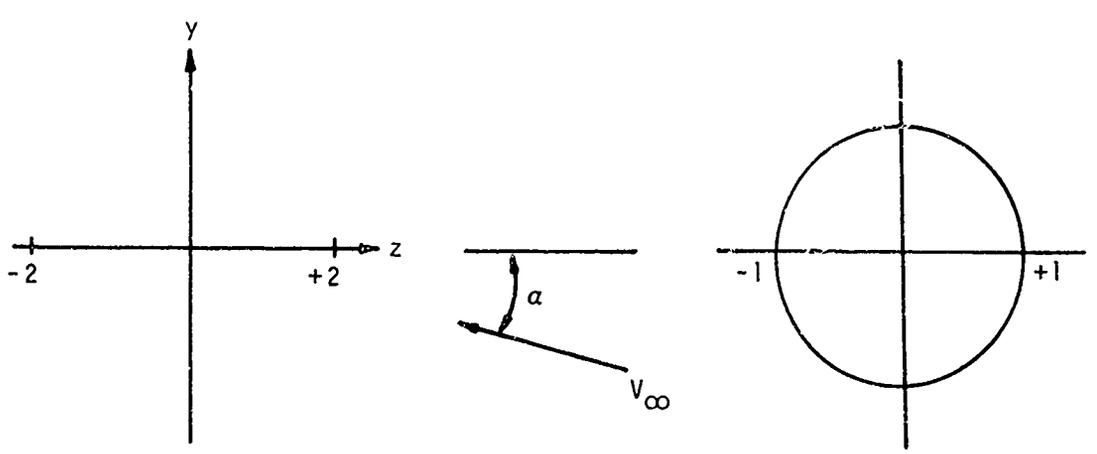

$$z = \zeta + \frac{1}{\zeta}$$

Figure 1. Conformal Mapping Coordinates in Transform Planes for the Two-Dimensional Analysis of Vortex-Lift Augmentation.

$$z = \zeta + \frac{1}{\zeta}$$

and the complete potential for the ζ-plane is found by adding the complex potentials of each of the elements (Reference 9) as follows:

$$w(\zeta) = V_\infty(\zeta e^{i\alpha} + \frac{1}{\zeta} e^{-i\alpha}) + i\, K_v[\ln(\zeta-\zeta_v) - \ln(\zeta - \frac{1}{\bar{\zeta}_v})$$

$$+ \ln\zeta] - m_j\,[\ln\,(\zeta-\zeta_j) + \ln(\zeta- \frac{1}{\bar{\zeta}_j}) - \ln\zeta] - m_v[\ln(\zeta-\zeta_v)$$

$$+ \ln(\zeta- \frac{1}{\bar{\zeta}_v}) - \ln\zeta] + i\, K_a \ln\,\zeta. \qquad (1)$$

The bar denotes complex conjugate and ζ_v and ζ_j are the vortex and jet positions in the ζ-plane (Figure 1).

Two kinematic conditions are available for solution of the problem: (1) as noted earlier, the flow appears to be attached in the neighborhood of the trailing edge, so that the Kutta condition of potential flow theory may be applied; (2) for the "actual" flow the vortex is stationary with respect to the airfoil; therefore, the potential flow must have a stagnation point at the vortex center when the singularities at that point are removed. The first condition generates one equation since the trailing edge of the airfoil transforms into a point on the real axis in the ζ-plane. In general the vortex location ζ_v, will be complex and will generate two equations. Thus, the following results,

$$\left.\frac{dw}{d\zeta}\right|_{\zeta=-1} = 0 = V_\infty(e^{i\alpha}-e^{-i\alpha}) + i\,K_v\left(-\frac{1}{1+\zeta_v} + \frac{1}{1+\frac{1}{\bar{\zeta}_v}} - 1\right)$$

$$- m_J\left(-\frac{1}{1+\zeta_J}\,\frac{1}{1+\frac{1}{\bar{\zeta}_J}} + 1\right) - m_v\left(-\frac{1}{1+\zeta_v} - \frac{1}{1+\frac{1}{\bar{\zeta}_v}} + 1\right) - iK_a = 0$$

or

$$K_a + \frac{2(1+\mathrm{Re}(\zeta_v))}{1+2\,\mathrm{Re}(\zeta_v)+|\zeta_v|^2}\,K_v = 2\,V_\infty \sin\alpha \qquad (2)$$

and

$$\left.\frac{dw}{d\zeta}\right|_{\zeta=\zeta_v} = 0 = V_\infty\left(e^{i\alpha} - \frac{1}{\zeta_v^2}\,e^{-i\alpha}\right) + i\,K_v\left(\frac{1}{\zeta_v} - \frac{1}{\zeta_v - \frac{1}{\bar{\zeta}_v}}\right)$$

$$- m_J\left(\frac{1}{\zeta_v-\zeta_J}\,\frac{1}{\zeta_v - \frac{1}{\bar{\zeta}_J}} - \frac{1}{\zeta_v}\right) - m_v\left(\frac{1}{\zeta_v - \frac{1}{\bar{\zeta}_v}}\,\frac{1}{\zeta_v}\right) + K_a\,\frac{i}{\zeta_v} = 0 \qquad (3)$$

where, in the last equation, the singular parts at $\zeta = \zeta_v$ have been removed. The real and imaginary parts of this equation are set to equal to zero so that, along with equation (2), there are three equations which may be used to determine K_a, K_v, and m_v, with m_J assumed to be known.

2.1.3 Limitations of the Model

The difficulties associated with this model are that leading edge separation is not represented, with the attendant large reduction in flow speed over the upper surface of the plate; and that a uniquely determinable position does not exist for the vortex. Regarding the second of these points,

if the condition, (refer to Figure 1 for definition of variables):

$$\left.\frac{dw}{d\zeta}\right|_{\zeta=\zeta_v} = 0 \tag{4}$$

is expanded mathematically with $\zeta_v = r_v e^{i\theta_v}$, the resulting equations involve r_v to the sixth power. This implies that at least one of the quantities, K_a, K_v, or m_v must be quite sensitive to vortex position, with all other conditions unchanged. This will be discussed further in the section on numerical solutions. It seems clear from flow visualization experiments that superposition of the several potential flows will not fully represent the true flow field due to the detached flow condition at the leading edge. The inclusion of a vortex feeding sheet from the leading edge to the vortex would allow a better approximation and, in addition, would provide a dynamic condition for uniquely determining the vortex position. In lieu of this complicating feature, a modified condition for stagnation at the vortex center is used. The region where the trapped vortex is finally established is otherwise a fully separated wake. Fortunately, results are available from surveys of the velocity distribution in the near-wake of a stalled flat plate, for a wide range of angle of attack above stall, indicating that the mean "cavity" velocity is about .1 V_∞ (Refs. 6, 10, and 11). Thus, in place of freestream velocity in equation (3) for vortex stagnation, the value

$$V_{cav} = .1\ V_\infty \tag{5}$$

is used herein. A similar reduction of upper surface velocity magnitude is computed more analytically in the three-dimensional solution because more complete knowledge of the "cavity" flow reversal properties is then available.

2.2 METHOD OF SOLUTION

Once a mass flow rate is established for the jet at a given angle of attack and free stream speed, the following procedure is used to obtain solutions. Since the "actual" location of the vortex is not known, a matrix of positions of the vortex must be computed and the resulting solutions for sink strength, vortex circulation, and airfoil circulation are then examined on physical grounds to determine the range of most reasonable values. While such analyses are valuable in providing an understanding of the nature of the flow interactions, they will not yield unique solutions since only one location of the vortex, unknown because the problem as posed is under-determined, corresponds to reality.

The two-dimensional representation of the jet as a source is intuitively appealing. However, the method for deriving an equivalent strength from three-dimensional data (Volume I of this report) is not entirely clear. For the results presented here, the entrainment rate from laser-doppler-velocimeter (LDV) measurements was used to compute the rate of expansion of the jet along its axis. This expansion then was equated to a source out-flow in cubic-feet-per-second, per foot of length. For C_μ = .46, the experimental value chosen for the most detailed theoretical calculations, the jet source strength is found to be m_J = 2.16. The actual value used for the following computations was rounded off to 2.0.

2.3 SAMPLE COMPUTER RESULTS

Figure 2 presents results for the jet positioned at .25c chordwise and at .075c above the airfoil. The vortex is placed at .10c, .15c and .20c chordwise. The position above the airfoil in percent-of-chord is the abscissa. For this case the outer free-stream speed is 100 fps. and α = 25 degrees. Clearly, K_a and K_v are not as sensitive to chordwise vortex position as is the vortex sink strength m_v. No criteria exist in the model to select the correct vortex position in this solution array; however, an argument can be made for bounding values on physical grounds. The vortex cannot have source flow at the core since this is an unstable (or non-sustainable) condition (Ref. 1). Therefore, a lower bound on vertical vortex position is indicated in Figure 2 for each chordwise position. The lower dotted line denotes the circulation strength at the given angle of attack for a fully stalled flat plate (Refs. 6 and 12), and it seems reasonable to assume that K_a will not be less than this value. The upper dotted line denotes the potential flow circulation limit for the airfoil alone. The lines above this level are the sums, $K_a + K_v$, for the three chordwise position solutions. It is interesting to note that circulation augmentation declines to zero for about the same vertical vortex position for which vortex sink strength tends to zero. Also, the total circulation is not very sensitive to chordwise vortex position, but the required vortex sink strength is quite sensitive.

The effect of moving the jet chordwise is demonstrated by Figure 3. Here the jet is located at .40c and the vortex at .20c, .25c, and .30c respectively. Comparing Figures 2 and 3, it is seen that a chordwise shift of the jet and vortex, keeping the relative chordwise spacing about the same, has little

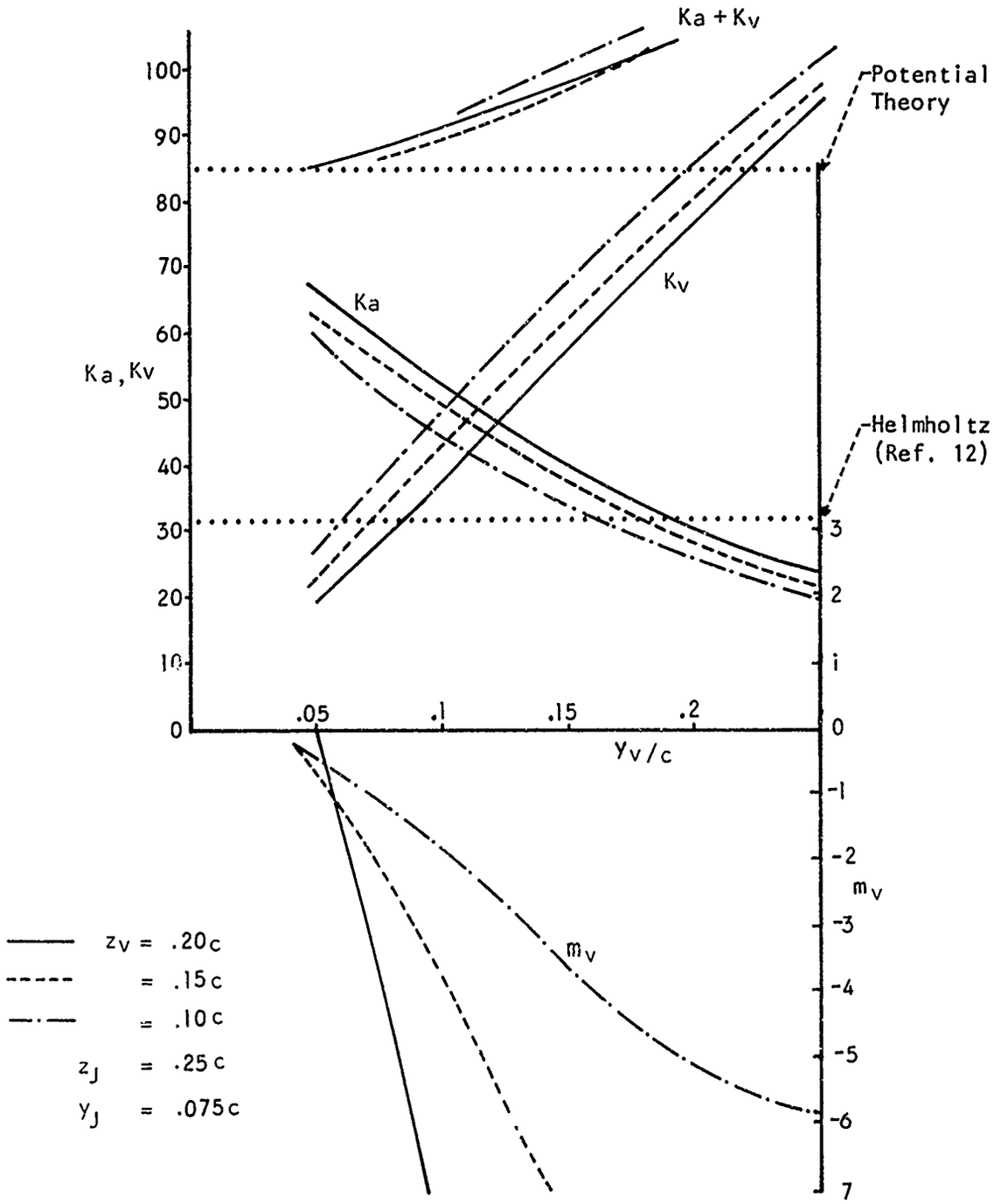

Figure 2. Singularity Strengths from the Two-Dimensional Analysis, α = 25°, m_J = 2.0, V_∞ = 100 f.p.s., Jet At .25c.

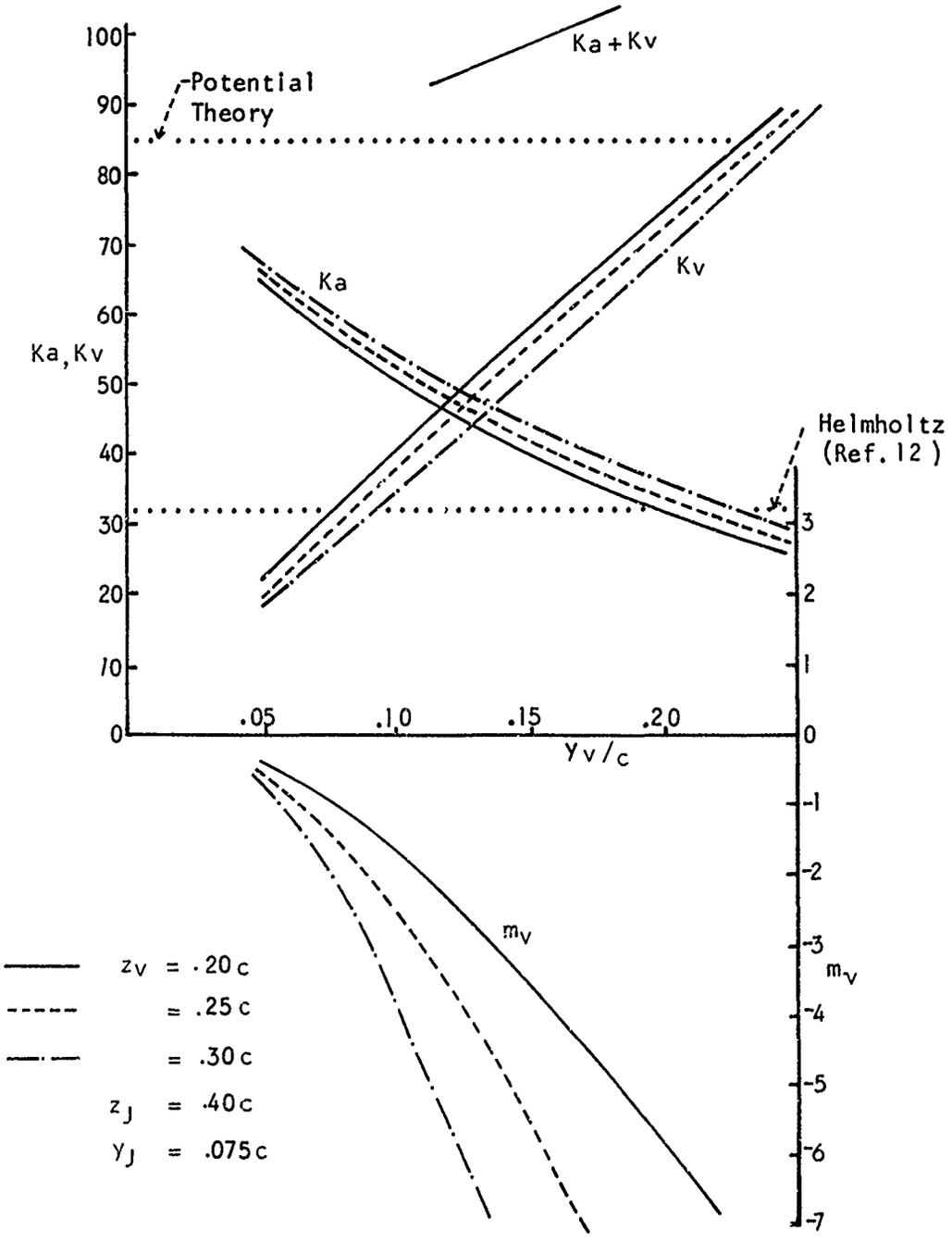

Figure 3. Singularity Strengths from the Two-Dimensional Analysis, $\alpha = 25°$, $m_J = 2.0$, $U_\infty = 100$ f.p.s., Jet at .40 c.

effect on the overall behavior with vertical spacing. In every case, placing the vortex and the jet closer together causes increased sink-strength in the vortex, a result to be expected physically since the jet axial flow induces axial core flow in the vortex.

Figure 4 presents a composite of C_ℓ versus α data. The dashed curve is the theoretical lift curve from thin airfoil theory. The measured C_ℓ for a flat plate is shown as indicated, and the curve resulting from the present two-dimensional model is also shown. In this case the jet is at .35c chordwise and .075c vertical and the vortex is at .25c chordwise and at .125c vertical. The jet strength is again $m_J = 2.0$, slightly lower than the equivalent value calculated from three-dimensional experimental data at $C_\mu = .46$. Comparison of the theoretical values for plain potential flow relative to that for vortex augmentation predicts, for example, at $\alpha = 25°$ a lift augmentation of about 12%. It should be noted that the lift in both cases is computed from circulation only. Thus, in the vortex augmented case, the lift coefficient is computed from

$$C_\ell = \frac{4\pi}{V_\infty c} (K_a + K_v). \tag{6}$$

Also shown in the figure are several two-dimensional values of lift coefficient as computed from experimental results for $C_\mu = .46$. To arrive at these values, the incremental-lift data due to blowing over the wing, as given in Figure 26 of the experimental part, Volume I of this report, was converted to equivalent two-dimensional values by use of the simple formula,

$$\Delta C_\ell = \frac{C_{\ell_\alpha}}{C_{L_\alpha}} \cdot \Delta C_L . \tag{7}$$

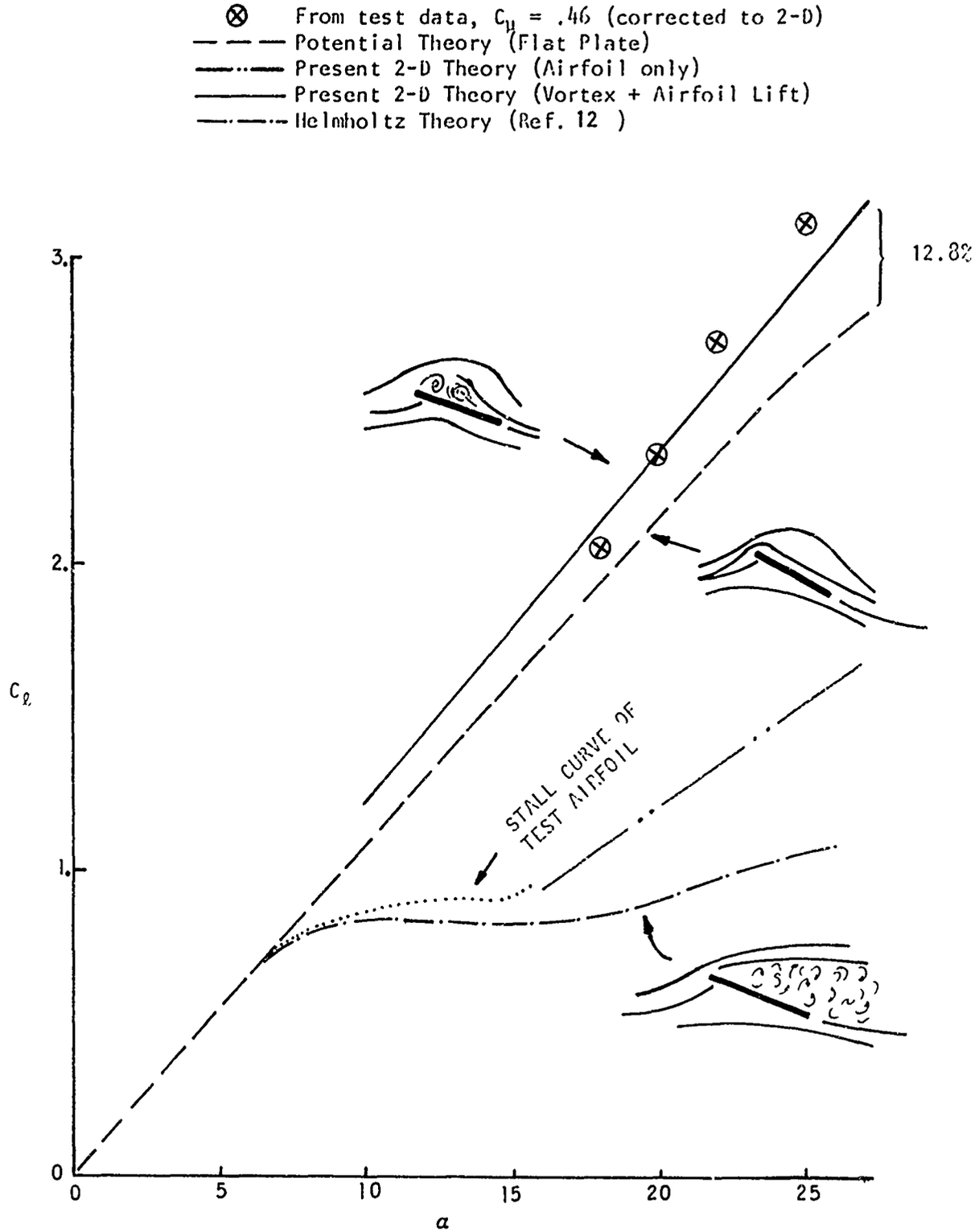

FIG. 4 TWO-DIMENSIONAL THEORY FOR VORTEX-LIFT CONTROL BY SPANWISE BLOWING - COMPARISON WITH TEST DATA

These increments were then added to the potential flow theoretical curve without spanwise blowing. Thus, it is implicitly assumed that the vortex increment for a flat plate would be the same as for the three-dimensional airfoil section. The agreement between theory and experiment is seen to be reasonable, but with a different slope in the data. This difference in slope is probably caused by the change in the actual position of the vortex relative to the airfoil surface as a function of angle of attack.

It is observed in smoke flow results that the vortex moves up relative to the airfoil with increasing angle of attack, and slightly forward. An indication of the movement of the vortex with angle of attack can be obtained from the data of Figure 4 by determining the vertical shift of vortex position required in order to give a theoretical value of lift matching the values derived from test data. The results for vertical vortex position versus α is shown in Figure 5, and an approximately linear relationship with α for the higher angles of attack can be seen for each value of m_J. The compatible variation of K_{V_α} for the vortex is given in Figure 6. Also, for the more optimum jet and vortex positions, shown in those figures and as indicated by the test results of Volume I, the vortex sink magnitude tends to be on the order of twice the resultant jet source strength.

Note that, for constant vortex heights, the magnitude of K_V changes very little in the two-dimensional solutions for a factor of 10 range of $m_J(C_\mu)$. This implies that optimizing the vortex location is of great importance for minimizing the spanwise blowing energy. The K_V's in Figure 6 are normalized to a reference value, $K_{V_{ref}}$, at a given vortex location,

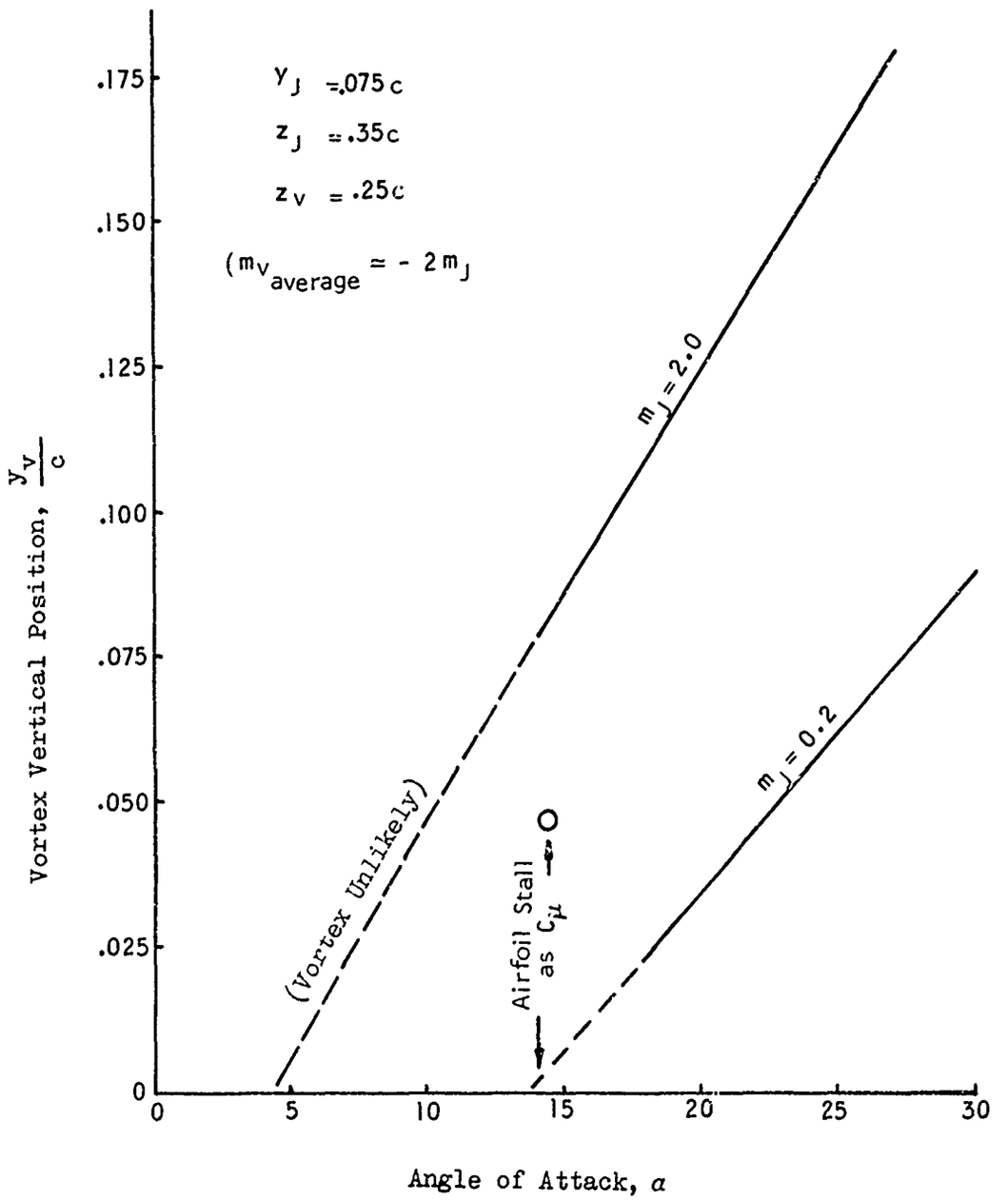

Figure 5. Derived Vertical Position of the Vortex from Two Dimensional Potential Flow

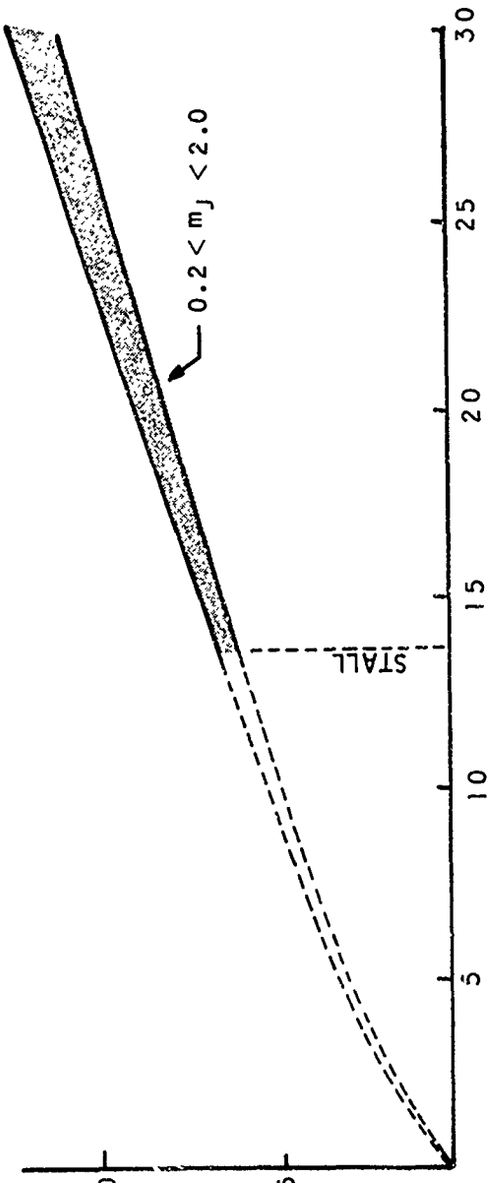

FIGURE 6 DERIVED CIRCULATION STRENGTH CHANGES WITH ANGLE OF ATTACK

y_v = .125c, and at an attitude α = 25°, which is sufficiently high that the flat plate results should apply to the tested wing, since full separation would be expected for both surfaces without any blowing momentum input. Figure 5 indicates a further reduction in y_v as the stall α is approached for a given airfoil "apparent" camber and thickness increase due to the jet displacement thickness over the wing. As C_μ approaches zero the actual incipient stall angle (14 degrees) for the tested airfoil (cf. Vol. I, Figure 29) is indicated, as expected. For any value of C_μ the flow tends to reattach below the natural stall angle, making discrete vortex formation unlikely as indicated in Figure 5. There is also an upper limit angle for each C_μ beyond which stall is bound to occur because of insufficient blowing momentum. These points will vary with configuration; but the preliminary analyses show that vortex burst at some station on the wing will indicate that this augmented-lift stall is being initiated. Fortunately, most test data (Refs. 3, 7 and 8) show that even past this point the maximum lift does not decline very rapidly.

Finally, the estimated circulation, K_{v_e}, corrected for finite wing camber, thickness and $m_J(C_\mu)$ as well as incidence angle, can be obtained by cross plotting (e.g., for m_J = 2.0) data in Figure 3 with incidence, α, from Figures 5 and 6 to determine the variation of effective sectional circulation, K_{v_e}, with vortex height, y_v/c as shown in Figure 7. At lower m_J's the reduced displacement thickness of the jet on the upper surface allows a smaller forward airfoil "cavity" depth for a given angle of attack, so the vortex has much less strength and is much closer to the surface than for higher jet momentum coefficients.

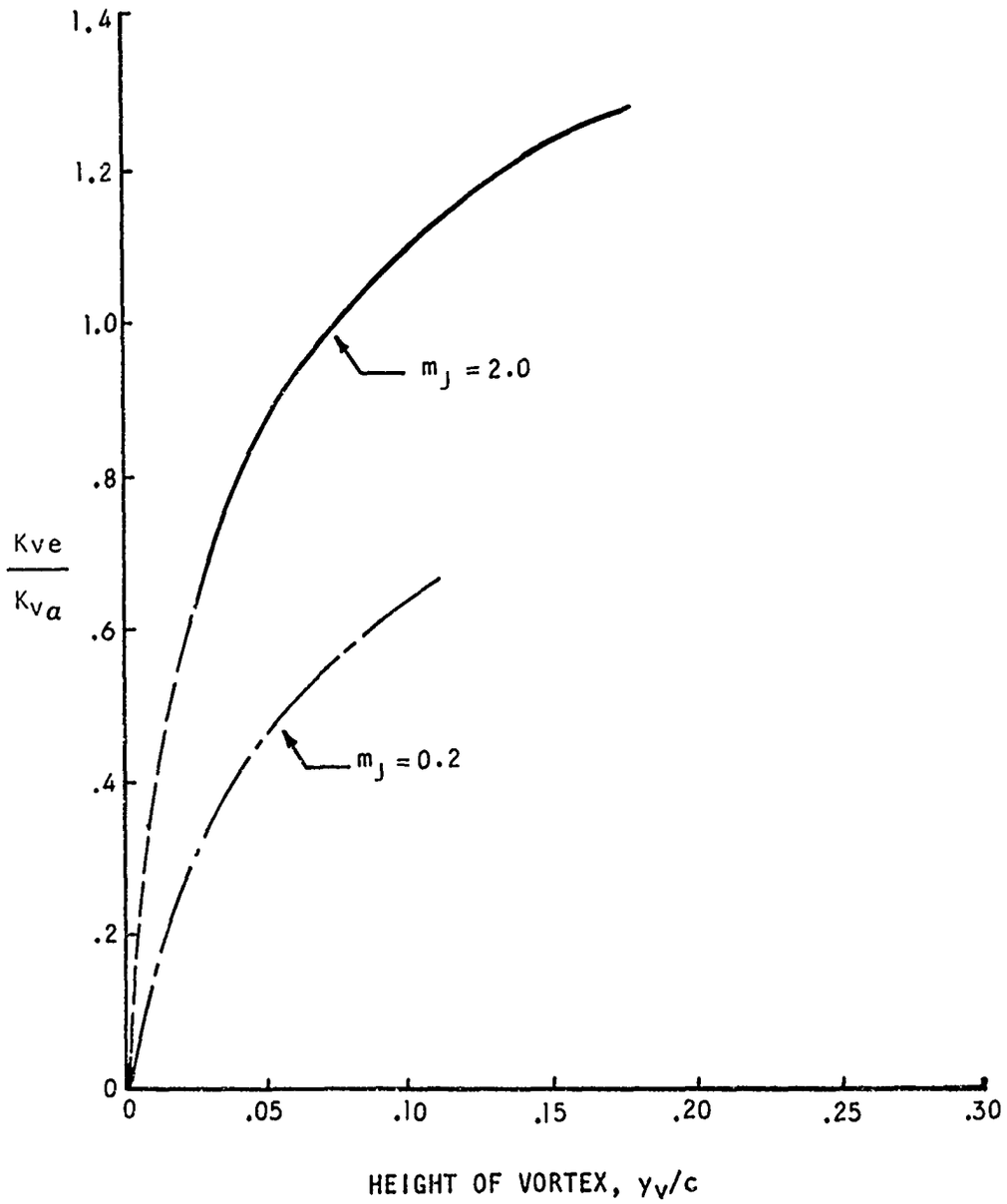

FIGURE 7 EFFECTIVE CIRCULATION CHANGE WITH VORTEX HEIGHT ABOVE THE WING SURFACE

Figure 7 thus can be used to obtain preliminary estimates of the two-dimensional K_v and vortex locations for input to the three-dimensional viscous analysis at any spanwise location in the vortex feeding sheet formation region. For other wing sections with significantly different leading edge radii or shapes, these predictions at lower angles of attack may not be very accurate since the average height of the vortex can be affected as discussed in Section 5.2.4, Volume I of this report. However, changes such as in thickness or camber of the wing section may be approximately accounted for if the natural ($C_\mu = 0$) incipient stall angle for the airfoil is known. In that case, the assumption is made that the vortex height at high incidence is not greatly affected; but the slope of the low C_μ curve in Figure 5 changes to conform with the intercept on the abscissa, which should be the stall angle for the new airfoil.

3.0 THREE-DIMENSIONAL THEORY FOR VORTEX-LIFT AUGMENTATION

3.1.0 INTRODUCTION TO THE THREE-DIMENSIONAL ANALYSIS

The analysis of spanwise blowing for vortex-lift augmentation must ultimately resolve the problem of regions of high energy jet and vortex flows in close proximity to a wing surface, as characteristic of many powered lift systems. Ideally, a mathematical model should include three-dimensional boundary layer interactions with the jet and vortex flow field. However, the present research objective was to obtain a physical understanding of the various flow phenomena involved. Detailed pressure measurements, flow visualizations of the leading edge and trailing vortex systems and LDV measurements of a jet issuing tangent to a plate, were used to gain an insight into the flow mechanisms required; but at present the relative importance of each of these flow fields can be established only by analysis until more detailed measurements are made, particularly concerning mixing in a cross flow. In the analytical model, the wing, the augmented leading edge vortex with a feeding sheet, and the jet centerline are represented by singularities consisting of source-sinks and vortex (lattice) distributions. Appropriate boundary conditions are imposed to determine the singularity strengths on the surface.

The principal empiricisms required are associated with the trajectory and enhancement of the spanwise blowing jet imbedded in the decelerated cross-flow region over the leading-edge of the wing upper surface. These formulas are taken with minor modifications from existing literature and discussed in Appendix A.

3.2.0 HYPOTHESIS FOR STABILIZATION OF THE LEADING-EDGE VORTEX

The lift augmentation phenomena described herein are most pertinent to wing angles-of-attack where highly separated flow from the leading-edge is normally present. Experimental evidence is sufficient to prove that, with spanwise blowing, a steady vortex will form in the lee of the separation region; so the analysis can proceed without further comment. However, an hypothesis can be made for the mechanism of leading-edge vortex stabilization, based on purely analytical arguments. Without rigorous proof, a brief argument is presented in the interest of possible better understanding of vortex stability.

Without spanwise blowing, at higher Reynolds Numbers, a wing experiences buffeting caused by quasi-periodic shedding of vorticity and breakdown into turbulence in the near wake. The methods of Refs. 1 and 6 have been proven to be capable of predicting the dominant spectral frequencies in the wake. In particular, the Strouhal frequency and its harmonics are derived in closed-form using the Navier-Stokes equation as summarized from Reference 1 in Appendix B. The solution is shown to be largely dependent upon the Rossby number, R_o, (ratio of linear-to-angular momentum) and the Radial-inflow Reynolds number, R_N. From the form of the equation of fluid-dynamic motion, it is apparent that stable, but periodic vortex modes are predicted when R_N is negative, so that the outer vortical layers of the separation region supply net radial inflow in a sustained manner. Under natural conditions, the vortex will continue to grow until the core axial flow accelerates to a burst condition (Ref. 13), or until the wake pressure defect can no longer restrain the vortex, so that a fully separated wake forms with periodically shed vorticity.

However, spanwise blowing is known to prevent these previously described oscillatory conditions. To understand this, one must recognize that the transformed equation (Appendix B) will indicate stable formation and axial growth patterns if R_N is positive. This is only possible in the upper part of the "cavity" flow region, as sketched in Figure 8, where the outer vortical layers of the leading-edge feeding sheet begin to swirl in towards the vortex core. However, simultaneously the co-rotating jet induces velocities which oppose those just behind the vortex. This reverses the entrainment process at the vortex periphery, and could be interpreted as vortex radial outflow. The mechanism for stabilizing the outer vortical layers, and preventing the periodic form of vortex shedding is thereby provided. As discussed in the two-dimensional analysis, the jet also acts as a source, providing flow toward the inner core of the vortex. This two-fold character of the jet is also described in Section 5.3.1, Volume I by using test observations on the high spreading rate at the core of the spanwise jet. These lateral-spread, wall-jet velocities combine with the feeding sheet elements over the wing surface, as observed in Figure 9(a), to entrain mass and momentum into the underside of the vortex. The jet thus augments the vortex core strength in a two-dimensional sense. In tests, however, it has been observed that excessive jet velocity can blow the vortex off the wing. Therefore, an equilibrium must be established wherein the detrainment (outflow) from outer vortical layers must balance the entrainment (sink effect) at the vortex core. Three-dimensionally, then, it is probable that there is a net reduction in the amount of fluid which would otherwise accelerate into the core and spiral out the vortex axis. This also explains the delay in vortex burst, caused by spanwise blowing, until the vortex curves aft to coalesce with the flap outer-edge or wing-tip vortex.

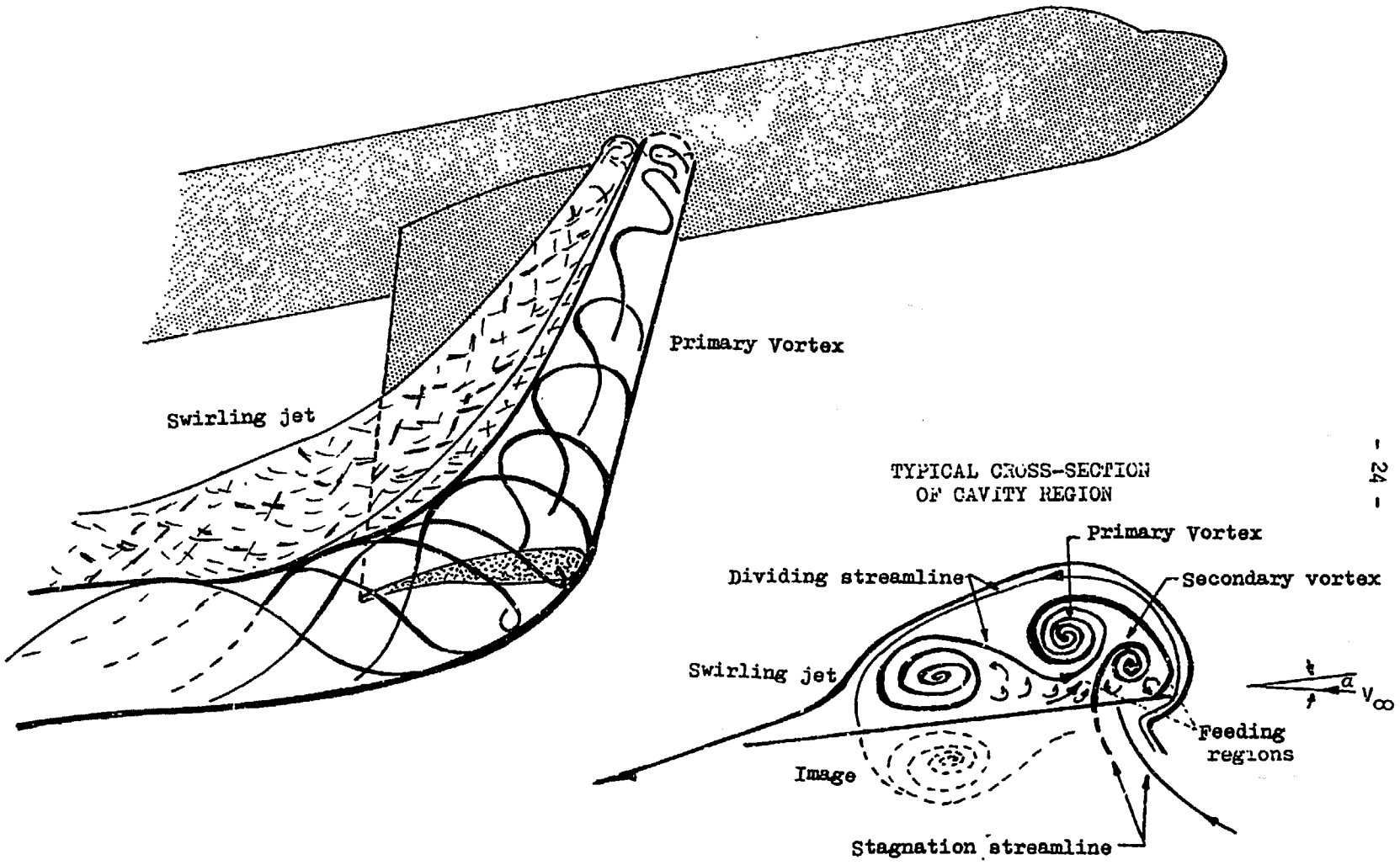

FIG. 8 OBSERVED PHYSICAL DESCRIPTION OF VORTEX LIFT CONTROL
(With full leading edge separation)

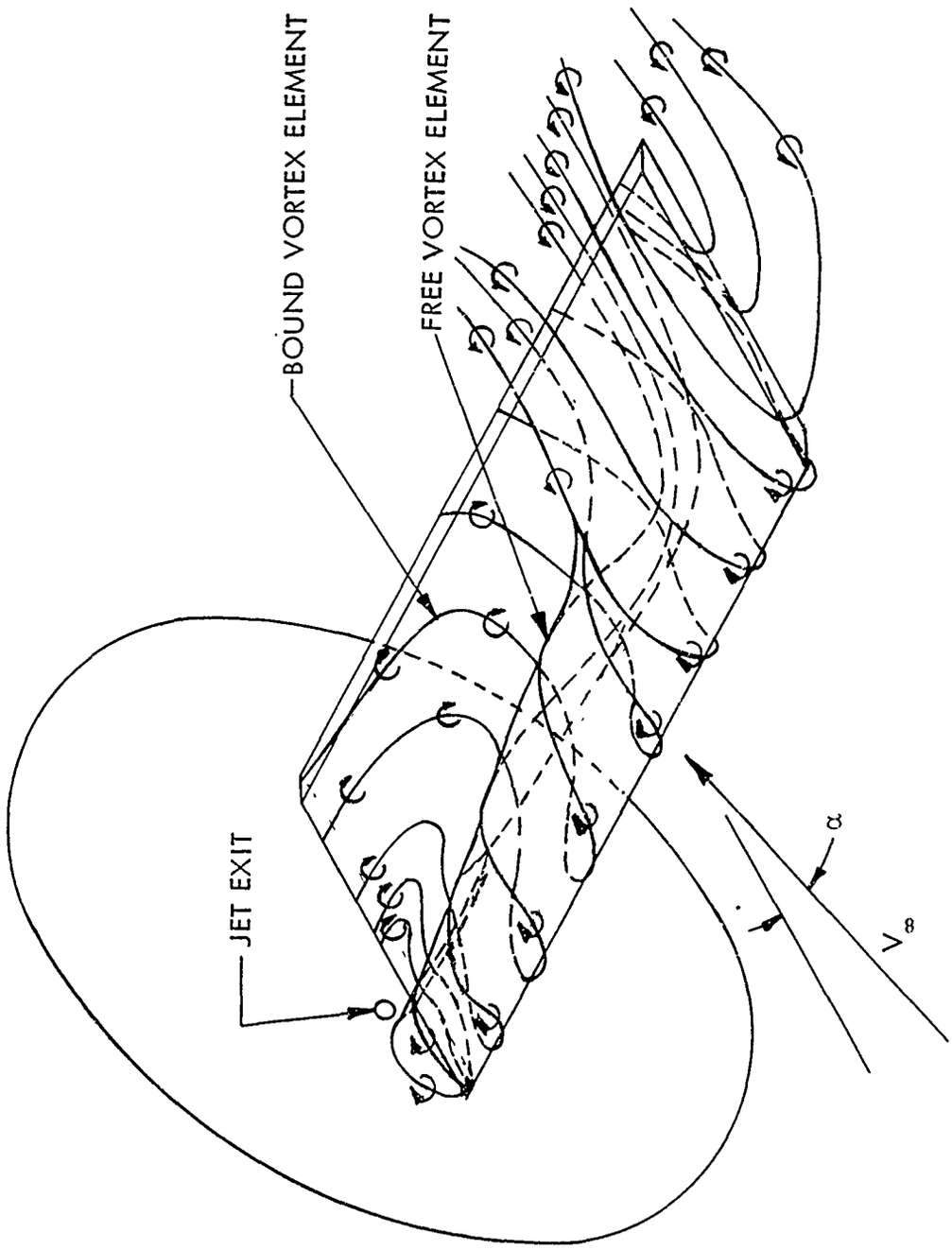

FIGURE 9(a) LEADING EDGE VORTEX LIFT CONTROL FROM TEST FLOW VISUALIZATION AT $\alpha = 14°$ (REF. 3)

The variation of vortex strength caused by increased entrainment in the mixing region is tractable by a method similar to that of Owen (Ref. 14), where the hard core is bounded by a finite annulus characterized by a time-dependent turbulent shear stress and the cascading of energy with frequency. This will be discussed in more detail in a later section on three-dimensional stability and viscous effects.

The form of equation used in Reference 1 for axial motion is probably not the most suitable for aperiodic flows where the leading-edge vortex is growing rapidly and approaching burst conditions. Also, the axis of the jet, and hence the vortex core, assumes a rearward trajectory on the wing surface because of the high local crossflow velocity. The general problem of a free jet penetrating a cross-flowing stream has received much study recently (Refs. 15, 16 and 17), but modifications to account for skewed impingement tangentially on a lifting surface are derived semi-empirically herein since no suitable analytic methods appear to be available.

3.3.0 OBSERVATIONS ON THE JET-VORTEX INTERACTION

3.3.1 Background Analyses and Tests

Reference to Figure 8 which was deduced from current experiments, shows in more detail how the primary vortex and the jet interact beneficially. Although some approximate solutions are available for either a jet in a cross-flow (e.g., Refs. 15 and 18) or for a viscous vortex forming in a near-wake (Refs. 1 and 5) or leading-edge separation region (Ref. 6), no solutions are available for a combination of these two issuing coaxially from a wall

(fuselage) and parallel to a surface (wing or flap). The Laser Doppler Velocimeter (LDV) measurements shown in Figure 11 of Volume I indicate that the jet velocity profile behaves much like a wall jet past the under-expanded region where Coanda type reattachment occurs. Visual evidence consisting of photographs of the jet erosion pattern over the upper surface during the LDV tests, reveals that the jet spread angle γ is about 4 times larger than that for a free jet, largely due to increased entrainment due to mixing with the rather thick, decelerated inner region of the boundary layer. A purely theoretical approach to describe such a complex, mixed flow region is beyond the scope of the present work. Detailed numerical solutions for wall-jets may be conceptually possible but the cross-flow and vortex and boundary-layer viscous terms would require a higher order theory. For the present purpose, a more intuitive formulation of the problem is employed to test the validity of the hypothetical flow mechanisms above the wing surface. Direct measurements to substantiate the velocities in this region must await tests using a backscattering laser-doppler or similar, non-interfering measuring system. Flow visualization has been helpful, but only the surface pressure measurements are quantitative. Thus, a semiempirical descriptive analytical model is used, calling upon available formulae whenever possible. The flow augmentation observed, however, indicates that the coefficients in such formulae are likely to need modification.

A literature survey has been made on the aforementioned topics, and a summary of those semi-empirical formulae applied herein is given in Appendix (A). Detailed justifications for each equation selection are not always given since in many cases alternative expressions are available, but the

differences in numerical results from a variety of references are considered minor, in most cases.

3.3.2 Jet Trajectory

Two primary assumptions are made. First, the presence of an image-plane due to the jet over the wing upper surface would cause some jet/vortex cross-sectional distortion (e.g., Ref. 18), but this is considered to be a higher order effect, so the variation of maximum axial local velocity, U_m, and the trajectories of a circular jet issuing from a vertical wall in a cross flow are assumed to apply in basic form. It is recognized that such a jet forms a plume consisting primarily of a pair of counter-rotating vortices which curve towards the mainstream direction. However, it is observed in the case of spanwise blowing, conceptually shown in Figures 8 and 9, that only one swirling jet issues in close proximity to the wing upper surface, but curving aft behind the leading edge vortex. As the jet profile develops in the spanwise direction, its characteristics, revealed by the preliminary LDV measurements, approach those of a wall-jet. The upstream, spreading component of velocity is terminated by a dividing streamline, separating the jet and vortex, yet revealing a path for the jet lateral velocity components to provide mass flow into the core of the primary vortex.

Thus, for a reasonable fluid dynamic analogy, the assumption must be made that the counter-rotating partner of the swirling jet is imbedded in an image plane formed by the wing upper surface as sketched in a cross-section of Figure 8.

3.3.3 The Leading-Edge Vortex

For a finite wing leading edge at high angle of attack, a feeding sheet forms somewhat as sketched in Figures 8 and 9(a). The data of Reference 3 gives substantiation of the assumption that the vorticity emanating from the wall (fuselage) region of jet formation curves forward over the upper surface, under the jet and "unbound" vortex and then is abruptly turned upwards at a fairly sharp angle. The curved sheet is approximated by a straight vortex-element sheet as sketched in Figure 9(b). The vortex elements are assumed to pass from the leading-edge to the primary vortex center in the manner assumed by Brown and Michael (Ref. 19). However, much improvement in results is obtained, e.g., for delta wings, using this greater detail of the formation region over the wing surface. A sample comparison of this method, for $C_\mu = 0$, with that of Polhamus (Refs. 20 and 21) for an aspect ratio 2.0 delta wing is shown in Figure 10. The agreement in lift partially substantiates the selected feeding sheet arrangement.

For a surface of infinite extent, a wall-jet tends to accelerate in the favorable pressure gradient created under a vortex of proper sign, as exists in Figure 8, but it may not greatly affect the strength of the vortex above the surface. The test data (Figure 10 of Volume I) indicate that normally the jet spreads at a much greater rate than does a free jet, probably due to surface friction effects and entrainment with a highly turbulent boundary layer. In this case, however, the presence of a strong feeding sheet at the wing leading edge will decelerate the forward lateral-spread component of the "wall-jet" abruptly, eventually resulting in a streamwise separation profile near the surface and a conversion of its vorticity in the process. Some acceleration of the feeding sheet velocity must occur as the jet velocity is turned upward approximately normal to the free stream direction.

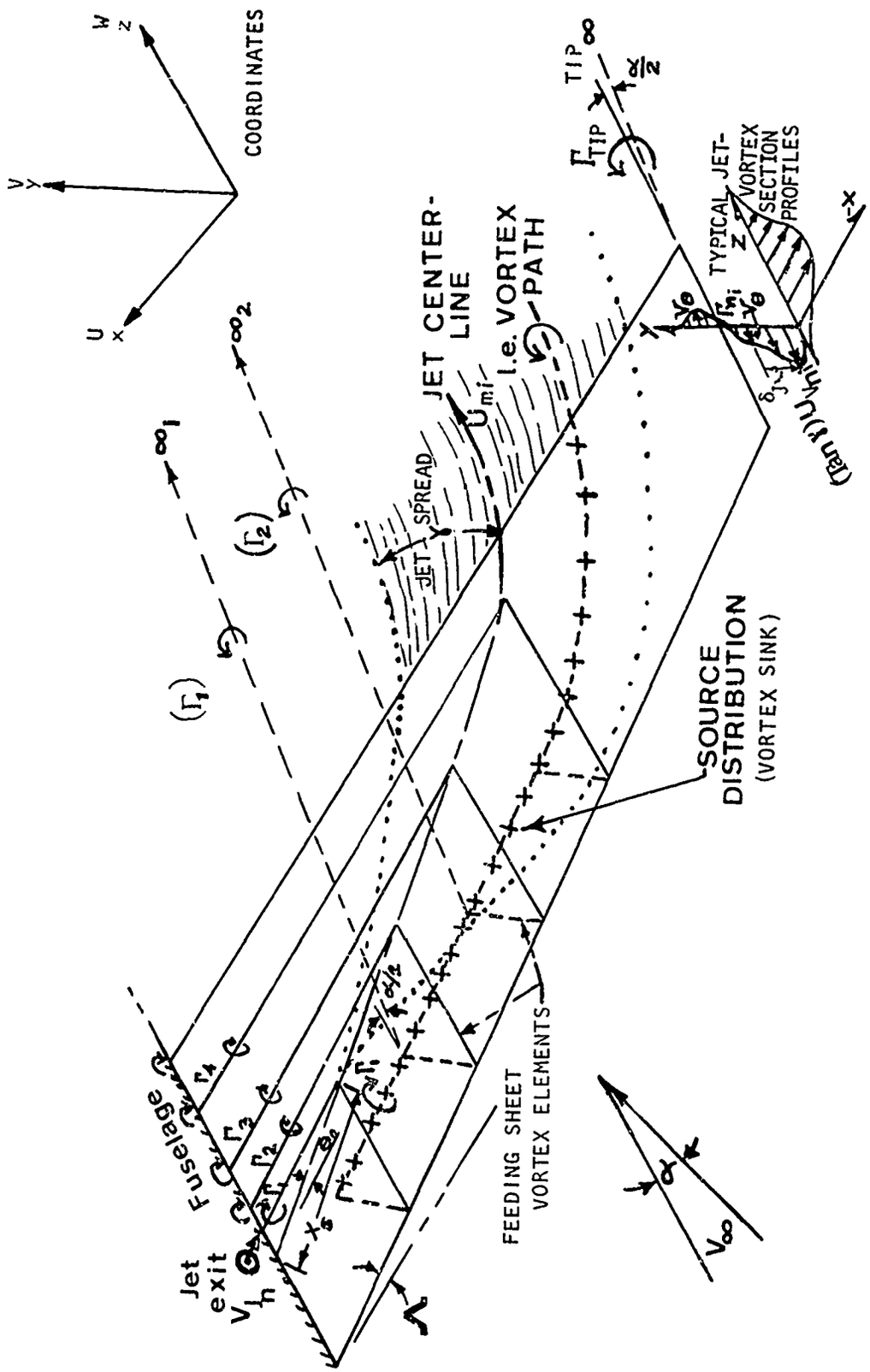

FIG. 9(b) LEADING-EDGE VORTEX LIFT - CONTROL WITH VORTEX-LATTICE AERODYNAMICS

KEY: (Leading edge vortex lift is in all $C_{L_{TOTAL}}$ values).

⊙ Present theory with $C_{L_{Potential}}$ including leading edge vortex induced velocities.

⊡ Present theory using $C_{L_{Potential}}$ without induced velocities from a feeding sheet.

—— Polhamus' theory (Ref.21) using $C_{L_{Potential}}$ from lifting surface theory.

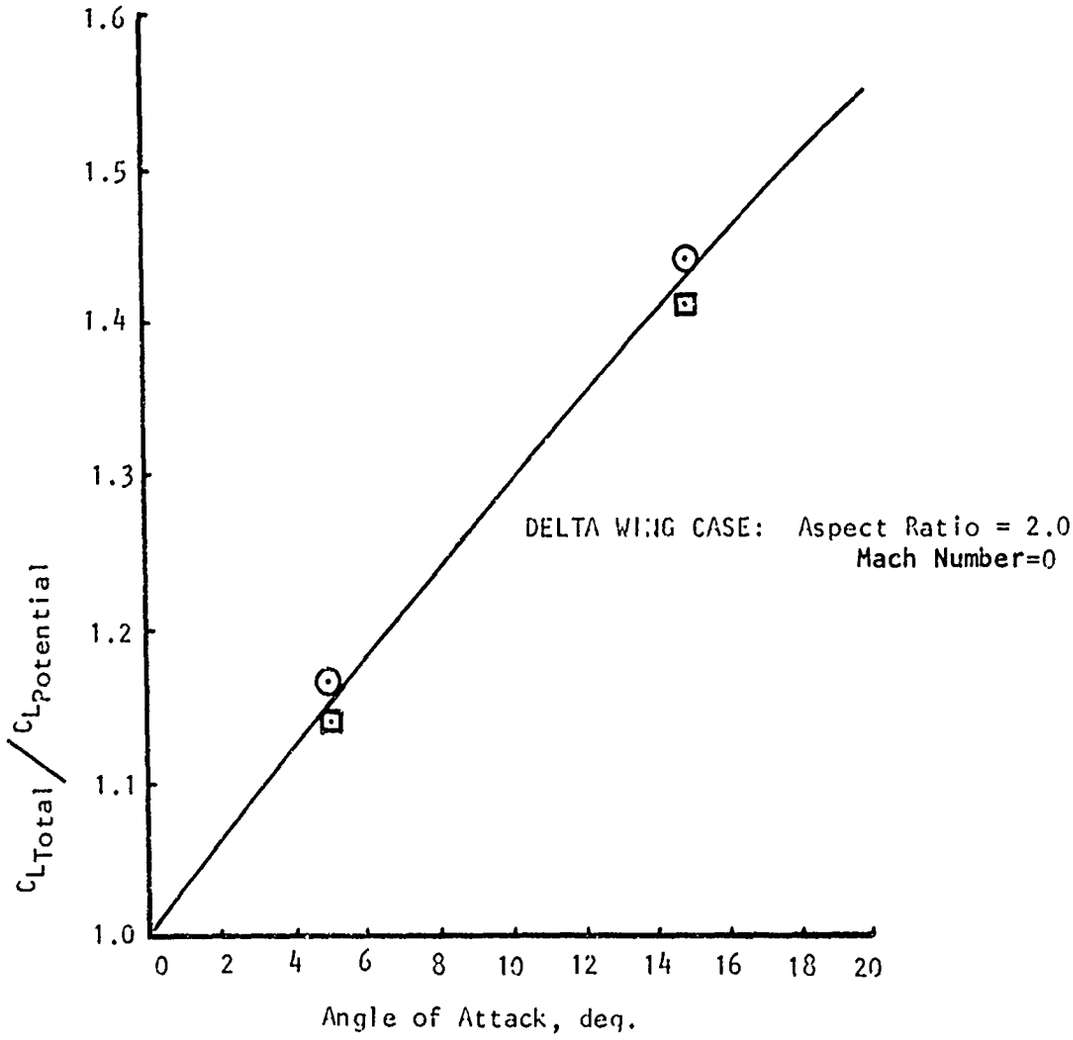

FIG. 10 COMPARISON OF LEADING-EDGE VORTEX CONTRIBUTION TO TOTAL LIFT USING A DELTA WING CASE FROM PRESENT THEORY FOR COMPARISON WITH THAT FROM POLHAMUS' THEORY FOR VARIOUS FEEDING SHEET AND POTENTIAL THEORY ASSUMPTIONS ON NORMALIZATION.

Concurrently, as described in Polhamus' leading-edge suction analogy, Refs. 20 and 21, the thrust force of this turning across the feeding sheet region results in momentum exchange causing a lift increment of equal magnitude. The vorticity involved is converted to added circulatory lift by augmenting the strength of the leading-edge vortex suspended in the low pressure region ahead of the jet and behind the feeding sheet. The simplifying assumption is made that only the positive (lift-contributing) increment of the lateral jet profile circulation need be considered in estimating the vortex augmentation, $\Delta\Gamma_J$.

3.3.4 Secondary Vortices

Presumably the negative vorticity components contribute to the formation of many turbulent secondary vortices in a highly viscous region very near the base of the feeding sheet. Here, wind tunnel tests indicate likely presence of one or more small, counter-rotating secondary vortices forward of the primary lifting vortex as sketched in the sectional view of Figure 8. Probably, a series of such minute eddies dissipates the energy of the lower side of the wall jet profile.

3.4.0 WALL-JET VORTEX PROPAGATION AND DECAY

3.4.1 Leading-Edge Vorticity Estimation from Jet Profile

The LDV measurements, Figure 13 of Volume I, indicate that the part of the wall-jet profile $U_m(x,y,z)$ above the maximum velocity point, Δy_m, (adapting terminalogy from Ref. 17) can be approximated by a straight line. Using the coordinate system in Figure A.1 of Appendix A, commonly accepted for a

jet in a cross-flowing stream (Refs. 15 and 16), the linear portion of the lateral jet velocity profile just beneath the vortex axis may be expressed approximately as

$$\left.\frac{dw}{dy}\right|_{z_{v_{ni}}} \simeq \frac{U_{v_{ni}}}{\delta_J} \tan\gamma \cos\theta_i \qquad (8)$$

where: (Refer to sectional sketch in Figure 9(b))

$z_{v_{ni}}$ designates the chordwise location of the n^{th} link of the primary vortex at the ith spanwise section (at x_i).

$U_{v_{ni}}$ is the jet axial velocity component at the above vortex location (see Appendix A).

γ is the jet spread half-angle (Figure 9(b)).

θ_i is the trajectory angle of the jet centerline, relative to the cross-stream direction, at section i.

and

δ_J is the effective depth of jet beneath the vortex at the dividing streamline (see Figures 8 and 9(b)), above the level Δy_m.

Since no data are available for a jet with these boundary conditions, the LDV measurements (Figure 11 of Volume I) are used to justify a value of $\delta_J \simeq 1.7\ D_o$ or approximately a constant times the nozzle diameter, D_o, as sufficiently accurate since the unaccelerated wall jet profile is vanishing near $\Delta y = \delta_J$. Note that D_o is an effective diameter (Appendix A).

Finally the vorticity must be integrated over each interval, Δz_n, from the wing leading-edge to the vortex chordwise position,

$$\Delta z_{v_{ni}} = z_{v_{ni}} - x_i \tan\Lambda \tag{9}$$

to yield the wall-jet vorticity available for vortex augmentation.

3.4.2.0 Vortex Augmentation and Decay

3.4.2.1 Augmentation

With $\vec{q}$ as the vector velocity across a line element $\vec{ds}$ the contour integral for the jet augmentation of vortex circulation, $\Delta\Gamma_J$ due to viscous spreading in the boundary layer at a section transverse to the vortex centerline may be expressed as a Stokes' integral:

$$\Delta\Gamma_{J_{ni}} = \oint \text{curl } \vec{q} \cdot \vec{ds}$$

$$= \int_0^{\Delta z_{v_{ni}}} \int_0^{\delta_J} \left(\frac{\partial w}{\partial y} - \frac{\partial v}{\partial z} \right) dydz \tag{10}$$

Within the accuracy of the jet profile data on the chordwise gradient in proximity to the stagnation streamline (Figure 8) the assumption may be made that $\left|\frac{\partial v}{\partial z}\right| \ll \left|\frac{\partial w}{\partial y}\right|$. For the higher blowing momentum coefficients, the bounding and stagnation streamlines remain at a nearly constant position relative to the wing leading edge. Thus, the jet is restrained from penetrating any farther forward, and it must expend its energy in entrainment with the vortex above the surface. The dominant gradient for this effect is $\frac{\partial w}{\partial y}$ although $\frac{\partial v}{\partial z}$ has implications with respect to vortex stability (burst) as will be discussed later.

Substitution of equation (8) into (10), with $\frac{\partial v}{\partial z} \simeq 0$, yields

$$\Delta\Gamma_{J_{ni}} = \int_0^{\Delta z_{v_{ni}}} \int_0^{\delta_J} \frac{U_{v_{ni}}}{\delta_J} \tan\gamma \cos\theta_i \, dydz \qquad (11)$$

Within the accuracy required for this purpose, it is assumed that $U_{v_{ni}}$ is approximately constant over each chordwise increment of integration, Δz_{ni}, principally influenced by only the n^{th} primary vortex link. Thus, to simplify the integration, $U_{v_{ni}}$ and θ_i are not considered as functions of y and z, particularly for the cases of most significance where the primary vortex is formed very near the leading-edge feeding sheet. The result may be expressed in the form,

$$\Delta\Gamma_{J_{ni}} \simeq U_{v_{ni}} \left(z_{v_{ni}} - x_i \tan\Lambda\right) \tan\gamma \cos\theta_i) \qquad (12)$$

This equation provides an estimate of the increase in circulation above that predicted by the 2-dimensional theory ($2\pi K$) which is used as the starting value for the vortex at the first inboard wing station beyond the under-expanded jet distance, x_s, from the fuselage sidewall or nozzle. At each spanwise station, x_i, the cumulation of circulation increments from the primary vortex links, given by equation (12) is added to the two-dimensional values.

3.4.2.2 Vortex Decay

It was found that for the above rather high vortex strengths the vortex "ages" rather rapidly according to Professor Owen's theory (Ref. 14), as described in Appendix A. Previous successful experience with this metnod over a wide Reynolds Number range, (Ref. 25), encouraged its application herein. The time varying turbulent eddy viscosity resulting therefrom decays

the vortex strength in a somewhat linear manner to values typically 1/3 of those predicted by the two-dimensional potential theory. An iterative calculation procedure is thus indicated; but it was found that the rule-of-thumb first estimate of the reduced vortex strength and trajectory variations resulted in convergence for practical purposes in one or two iterations.

3.5.0 THE VORTEX-LATTICE/SOURCE-SINK PROGRAM

3.5.1 The Computer Simulation Model

The above equations, along with the semi-empirical formulations for jet and vortex growth, entrainment, and viscous dissipation found in Appendix A, provide the basic elements necessary to simulate vortex-lift control as depicted in Figure 9(b). However, the application of such elements in a vortex lattice program (e.g. Refs. 15 and 22-24) for powered/augmented lift analysis, as delineated in Figure 11, is more complex and extensive than was originally intended in this research program. The phenomena are so highly three-dimensional and viscous that the limitations of the two-dimensional theory became evident early in the analysis. Nevertheless, the 2-D theory is essential to provide starting conditions for logical vortex locations and strengths and source/sink effects.

Ideally, the singularity distributions from the jet, vortex feeding sheet and lifting surface should all be included simultaneously in the computation of mutual induction effects while satisfying the flow tangency boundary conditions at collocation points throughout the wing. This objective is attempted in the final steps as shown in Figure 11; but certain non-linearities present in such a viscid/inviscid interaction process, particularly in the event of vortex burst, imply that assumptions of superposition must be made

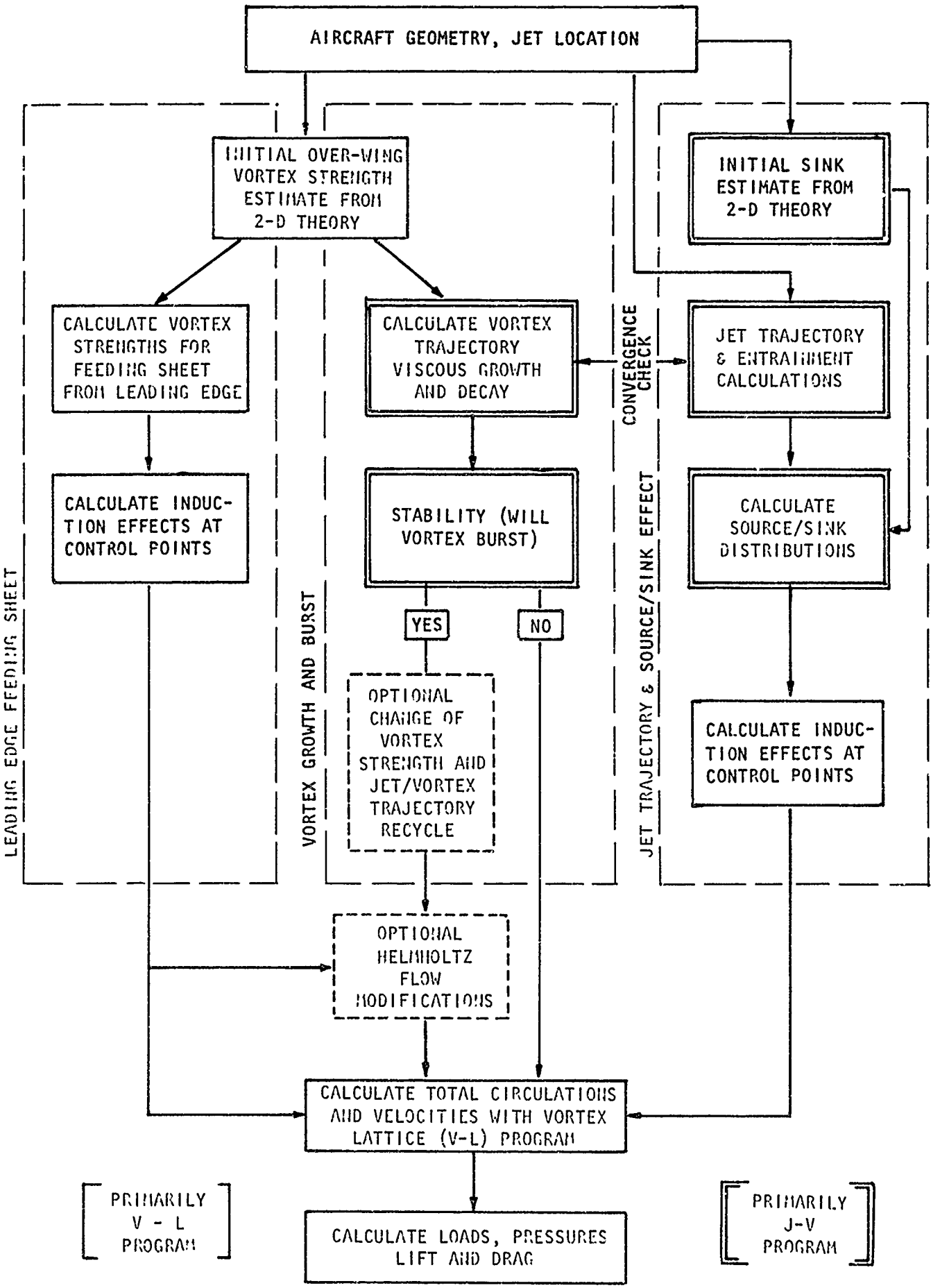

FIGURE 11. VORTEX-LIFT CONTROL FLOW DIAGRAM OF THREE-DIMENSIONAL VISCID AND INVISCID COMPUTER PROGRAMS

at intermediate steps in the program calculations. Hopefully, iterations on all or part of the steps in Figure 11 compensate and lead to minimum errors. For example, the jet trajectory is dependent upon the mean upper surface crossflow velocity. This is, in turn, related to the vortex strength variation since the circumferential velocity creates a backflow component tangentially, close to the surface (e.g., see the Figure 8 typical cross-section). But the vortex strength depends on the jet strength and entrainment variation in the boundary-layer/"wall-jet" region; so an iteration is indicated in the flow diagram of Figure 11 with a convergence check on the jet and vortex paths. If the leading-edge vortex strengths vary significantly from those for previous steps, the feeding sheet is modified accordingly, and new induction effects are calculated to enforce the boundary conditions again.

Fortunately, the pressure coefficients did not vary significantly on the average, so few iterations were required for the optimum cases studied. In this respect, the program is not sensitive to the distributed sink strengths except at low attitudes where close proximity of the unbound vortex elements to the wing surface induces some locally high velocities. Such cases are not optimum for vortex lift augmentation, and thus should not be of great concern. However, the problem was found to be much alleviated by applying smoothing techniques or spline curve-fitting techniques to the most severely fluctuating induced velocities in the previous iteration before proceeding to the next simultaneous equation solution. Such methods are recommended (Refs. 27 and 28) where finite-element, singularity-distribution methods are employed. The solution convergence is much more rapid for optimum smoothing (Ref. 29), and the mathematical possibility of introducing non-unique solutions is minimized.

In the future, a solution is conceptually possible by a more direct iterative approach combining the time/spacially varing lattice of Ref. 15 with time-dependent turbulent boundary layer methods (Ref. 30); but the semi-empirical method proposed herein is more feasible at this time since it employs approximate, closed-form expressions for viscous and entrainment processes along with the well known and proven vortex-lattice techniques. More detailed descriptions of the latter programs are given in References 15, and 22 through 24.

3.5.2 Input Conditions for the 3-D Solution

The program sequence is shown in the flow diagram of Figure 11. The coordinate locations for each panel of the wing, flaps, or other portions of the airplane are computed automatically in the vortex-lattice (V-L) computer program by merely specifying the corner points of each major section which does not have either chordwise or spanwise discontinuities. Thus, it is convenient to first make a V-L run at the desired attitude, α, to obtain the coordinates of the load points, through which the spanwise bound vortex link of each panel passes, and the collocation (control) points where the exact tangency boundary conditions are imposed in the matrix solution. This provides a check against the unpowered lift, or potential flow solutions. Also, these coordinates are required as input for the solution of the viscous jet-vortex (J-V) equations (Appendix A) in a cross flowing stream.

The chordwise coordinates and initial strengths of the vortex and jet for a given C_μ and α are specified from the two-dimensional solution at a characteristic spanwise station. This may be either at the wing root or at any position for outboard spanwise blowing. The jet and vortex velocities and

trajectories are computed for as many nozzles as are present. The jet augmentation (equation 12) and viscous dissipation from Owen's theory, Ref. 14, are accounted for in obtaining an improved vortex strength variation, $\bar{K}_{n1}$, with span which is then input to the V-L program, properly accounting for the cross-flow trajectory of the vortex centerline. As discussed previously, the unbound, locked vortex feeding sheet is assumed to emanate from the fuselage wall and boundary-layer region by means of equally-spaced discrete vortex elements which are assumed to be bound in the surface parallel to the local sweep angle, and coincident with the nearest quarter-panel-chord bound-vortex leg to minimize potential interactions of two singularities in proximity to each other (e.g., see Ref. 15). These vortex links, having strengths consistent with the previously determined spanwise Γ variation, are then assumed to extend spanwise until they are turned forward by the backflow velocity components approximately beneath the jet or locked-vortex centerlines, as appropriate from the wing geometry and J-V trajectory printout. They are then swept forward to the wing leading edge and thence back up to the unbound vortex to simulate the leading edge feeding sheet represented somewhat in the manner of Brown and Micheal, Ref. 19. Continuity of vortex lines is ensured by allowing some of the local vorticity to be shed into the wake at an angle $\alpha/2$, based on experience with V-L methods, Ref. 22-24, and the remainder to propagate out the wing span and aft to eventually merge with the wing tip vortex.

The additional entrainment expected from the finite wing leading edge conditions seems to be derived naturally from the two-dimensional solution for the range of practical attitudes and momentum coefficients shown in Figure 5.

On the average, the vortex sink strength m_v varied less than plus or minus 25 percent from the relationship

$$m_v \simeq - 2\, m_J \qquad (13)$$

and the variation above stall was not consistently increasing or decreasing with α for the range of momentum coefficients, $.046 \leq C_\mu \leq .46$. Thus, within the accuracy of the two-dimensional assumptions, equation (13) was used as sufficient for starting conditions in the V-L program. The J-V program computes values of $d\varphi/dx$, volumetric mass flux change with wing span as discussed in Appendix A, and these can be used to obtain more accurate values for m_J if this is desired.

For a given C_μ, values of K_v versus α can be established for constant jet and vortex locations which are very much like those shown in Figure 6. However, based on earlier discussions in Figure 6 it is also necessary to account for the reduction in K_v with lesser values of y_v as shown in Figures 2, 3, and 7. As angle of attack decreases, the vortex clings closer to the upper surface, and the separation (cavity) region is smaller, so vortex strength reduces typically as shown in Figure 7. The usual procedure is to select an attitude such as 25 degrees, sufficiently above natural stall for a given airfoil that the vortex strength (then called $K_{v_{Ref.}}$) and height determined from the flat-plate theory will be adequate for a fully separated flow. Then the two factors from curves such as those in Figures 6 and 7 are both applied to unnormalize the K_v and y_v for lower values of α.

The J-V program has the option of computing the jet velocities out of a singularity distribution, but the "lumped parameter" distribution of these

sources was not available in an economical manner from any theory or tests; so an alternative procedure was devised using jet vector "supervelocities" from Appendix A formulas, multiplied by an empirical factor prior to application at grid collocation points, as discussed in the next section.

3.5.3 Solution Objectives and Modifications

3.5.3.1 Summary of Loads Computation Method - The purpose of the three-dimensional program is to combine the effects of jet-vortex interactions, along with vortex persistence and stability, to obtain the resultant velocities over an arbitrary wing surface represented by a vortex lattice. Thus it is possible to compute the incremental pressure coefficients, ΔC_p, associated with the jet and vortex source/sink systems, and with the vortex lattices for the wing and the feeding sheet.

In general, the total force at a local station on the wing according to potential theory can be expressed in the form,

$$\text{Total Lift} = \rho (V_{V-L} + V_S) (\Gamma_{V-L} + \Gamma_v)\Delta L \qquad (14)$$

where,

V_{V-L} are velocities which lie in vertical streamwise planes and are induced, at the load points, by the basic vortex lattice system system in the wing.

V_S are superposed velocities, in streamwise vertical planes, caused by feeding-sheet elements, by sources and by sinks in the field. (There is also a fuselage-body thickness correction included (Ref. 31), in most cases.)

Γ_{V-L} are the local circulations determined after all mutually-induced and all supervelocities have been applied at the collocation points. The effects of the feeding sheet are included explicitly.

Γ_{v} are the local circulations in the wing which join the leading-edge feeding sheet and ultimately form the separated vortex above the wing. These eventually trail downstream to infinity.

and,

ΔL is the cross-stream projected length of a given bound vortex element.

A difficulty is created by the cross-product terms of equation (14), since these imply that simultaneous solution of the inviscid (V-L) and viscid (J-V) equations is required to obtain mathematically consistent loads. The assumption is made that the iterative convergence tests are sufficient to satisfy the necessary compatibility and uniqueness conditions.

3.5.3.2 Semi-empirical Modifications to Surface Supervelocities for Reduced Crossflow - Experience with vortex-lattice methods reveals that the matrix of influence coefficients is adequately determined for most conventional wings by consideration of only the potential velocity field beyond the boundary layer. At most, a classical thickness and/or camber correction may be necessary to account for an effective wing thickness increase due to boundary-layer displacement thickness. In the case of "boundary layers" consisting of

thick wall-jet profiles, where velocity defects are significant at large distances from the wing surface, available literature does not indicate any simple correction that has been successfully tried. This situation is aggravated by the tangential velocity gradients, created by the unbound "leading-edge" vortex, which merge with the jet velocities as shown in Figures 8 and 9 at even greater distances in the separated flow region.

If an effective, mean upper-surface (cavity) flow velocity is defined as V_e, then we may express the cross-flow velocity ratio for the jet as

$$R = U_J/V_e \tag{15}$$

It already has been shown (Equation 5 and Refs. 6, 10 and 11) that the velocity in this region may be as little as 10 percent of the free stream velocity, V_∞ . Thus for a sonic jet, as found to be optimum in Volume I of this report,

$$R \gg 1 \tag{16}$$

A similar argument can be made for the ratio of the effective "streaming-flow" component, V_e, divided into the maximum wall-jet velocity at station i in the laterally spreading direction just beneath the n^{th} unbound vortex element, given as

$$\frac{U_{Vni} \cos\theta_i \tan\gamma}{V_e} > 1 \tag{17}$$

In that case it is shown in Reference 26 that only about 8 percent of the resultant jet velocity remains effective at the profile position equivalent to the boundary-layer displacement thickness. Similar factors are derived in

Reference 17. Thus, on a somewhat intuitive basis, the incremental contribution to the local pressure coefficient, caused by the effective "cavity" velocities over the bound legs of the vortex feeding sheet, can be computed by modifying that portion from Equation (14) as follows:

$$C_{p_{ni}} \simeq \frac{-2\pi\rho\bar{K}_{n_{ij}}\Delta L_{ij}C_w}{q\,S_{ij}}\left\{k_{ci}\left[U_{v_{nij}}\sin\theta_i + V_{e_{ij}}\right] + e_o V_\infty\right\} \tag{18}$$

where: q is the dynamic pressure; $\bar{K}_{n_{ij}}$ is the final augmented circulation strength of the n^{th} vortex element at span station i, and ΔL_{ij} is the corresponding bound vortex link length; and S_{ij} is the area of the wing lattice panel affected by $\bar{K}_{nij}$. The factors k_{ci} and C_W are required by a V-L representation because of the extreme differentials in effective outer/inner and upper/lower-surface, respectively, flow velocities. The k_{ci} adjusts for the effective velocity sensed by the bound-lattice network in the upper surface due to the velocity gradient normal to the surface in the cavity backflow region. This gradient is related to the depth of the cavity formation region, proportional to $\sin\alpha$, over which the velocity change occurs. If an "effectiveness factor" is defined, based on Ref. 26 data, as $e_o \simeq .08$, then

$$k_{c_i} \simeq e_o\left[(V_\infty - V_e)\sin\alpha\right]/V_\infty \tag{19}$$

and

$$C_w = \frac{\text{Average velocity over the upper surface}}{V_\infty} \simeq \tfrac{1}{2} \tag{20}$$

in the case of augmented lift with reattached flow over much of the upper surface.

The factor e_o is also applied in determining the effectiveness of the wall jet-like profile when it is penetrating the forward airfoil region of greater backflow velocity due to the vortex tangential component, $V_{\theta_{ni}}$. This amounts to a reduction in effective free stream cross-flow velocity, explaining in part the concluding results in Equations (5) and (15). The available empirical formulas only allow a mean cross-flow velocity, V_e, to be applied to the jet velocity and trajectory computations. However, as shown in Appendix A, after this initial approximate pattern is established, experience indicates that improved values of V_e can be obtained at each span station i by using the relationship

$$V_{e_i} = V_\infty \cos(\theta_o + \Lambda) - e_o V_{\theta_{ni}} \tag{21}$$

across the wing span. The vortex tangential velocity $V_{\theta_{ni}}$ at a distance $(r_{ni} + \delta_J)$ below the "locked" or suspended leading-edge vortex axis (refer to Figures 8 and 9) is approximated as,

$$V_{\theta_{ni}} \simeq K_{ni}/(r_{ni} + \delta_J) + K_{Jni}/r_{ni} \tag{22}$$

with

$$K_{ni} = \frac{\bar{K}_{nij}}{\bar{K}_{n1j}} K_{V_e} \tag{23}$$

and

$$K_{Jni} = \Delta\Gamma_{Jni}/2\pi \tag{24}$$

as the jet circulation augmentation from equation (12)

Finally, the vortex effective radius r_{ni} is defined in Appendix A along with a discussion of the viscid method for computing, $\bar{K}_{n_{ij}}$, the final circulation strength variation.

3.5.3.3 Jet-Vortex Viscous-Stability Effects - The J-V viscous effects program also computes vortex burst criteria as delineated in Appendices A and B. For wing stations past the critical stability points, highly turbulent, separated flow is predicted. Thus the values of C_p, lift and moment from potential theory must be modified. Fortunately, scientists at the Lockheed-Georgia Research Laboratory devoloped (in Reference 12) a modified Helmholtz theory more generally applicable to stalled lifting surfaces.

Basically, the method employs the procedure described in Reference 9; but it uses a modified upper surface suction pressure, logically deduced from known drag characteristics in the presence of extensive separated flow over airfoil sections. Similar crossflow drag concepts have been adopted successfully for nonlinear lift representation in References 32 and 33. The assumption is made that the revised average near-wake pressure applies in the separated, turbulent flow region created by vortex burst. Then the ratio of the Helmholtz lift to the potential lift, from Reference 12, is as follows,

$$H = \frac{9}{8} \sin(2\alpha)/(4 + \pi \sin\alpha) \sin\alpha \qquad (25)$$

This factor is multiplied times the $C_{p_{V-L}}$ from the potential, vortex- lattice solution as influenced by the appropriate supervelocities. At high angles of attack this method is remarkably successful as shown in Section 4.0, THEORETICAL RESULTS AND COMPARISON WITH TESTS.

At lower angles of attack, when vortex burst occurs in the stall-transition region, an improved correction can be obtained by taking the ratio of Helmholtz-to-potential-flow lift directly from Figure 4 at the given angle. At high incidence, when the jet and vortex are swept aft quite severely

because of too little mass-momentum injection, the primary vortex may be weak and too small to prevent a large separation region from forming (due to secondary-vortex/turbulence) forward of it and aft of the leading-edge. Preliminary calculations at $C_\mu = .115$ indicate that it is pertinent to apply the modified Helmholtz factor in this region, as well as outboard of burst-critical stations, prior to the addition of the incremental pressures, ΔC_{p_v}, from the vortex feeding sheet analysis.

For some cases at higher incidence and C_μ, the Owen's time/spacially varying eddy viscosity formulation (Refs. 14 and 25), combined with the Rossby number stability criteria (Appendix A and Ref. 34) seems to be capable of predicting some conservation of angular momentum after burst occurs. As the aging process re-initiates, the vortex again re-coalesceses into a coherent rotating fluid mass. If this occurs on the wing, it is possible that the V-L computed pressures are again satisfactory past the region of burst recovery.

Additional confidence is gained in the viscous methods employed by comparing the calculated time-dependent turbulent eddy viscosity ν_T with available test data and with recent, more sophisticated methodology. Figure 12 shows that the turbulent eddy viscosity ratio, ν_T/ν, predicted herein agrees favorably with wing vortex wake data summarized in Ref. 35 as a function of vortex Reynolds Number, Γ/ν. The analytical point is for the 8-degree angle-of-attack case where the leading-edge vortex quickly leaves the wing upper surface, and penetrates about one wing span into the near wake, just before vortex burst occurs. Similarly, comparisons were made with wake vortex radius growth predictions using boundary layer turbulent shear-stress concepts by

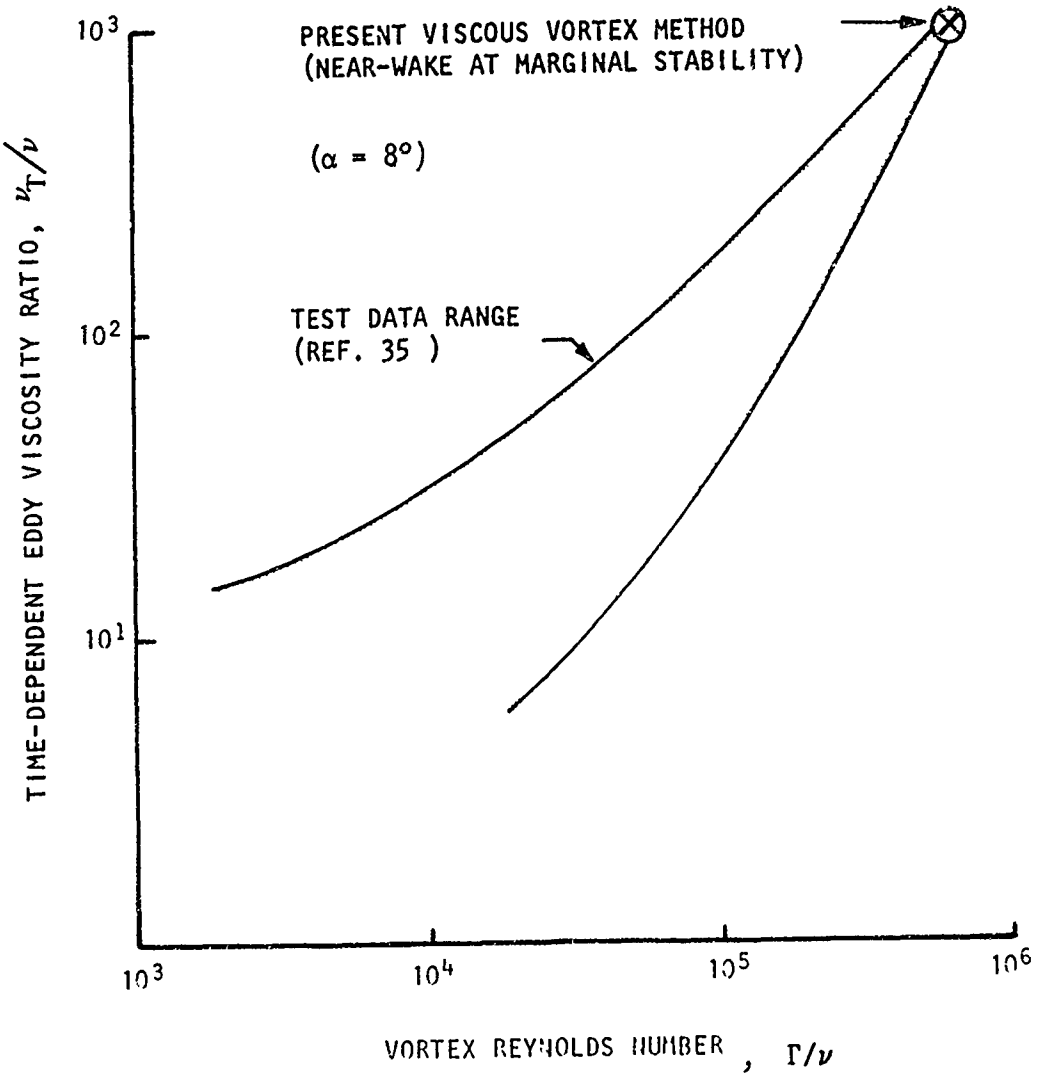

Figure 12 COMPARISON OF THEORETICAL AND EXPERIMENTAL EDDY VISCOSITY DATA

Dr. J. F. Nash (Consultant to Lockheed, Ref. 36). Again, qualitatively good agreement was obtained on intermediate wake vortex growth rates since both methods showed similarly significant differences from the classical "square-root-of x" variation, depending upon model-scale effects.

4.0 THEORETICAL RESULTS AND COMPARISON WITH TESTS

4.1.0 LOW INCIDENCE RESULTS OF VORTEX--LIFT CONTROL THEORY

A distinct difference in the character of jet-vortex interaction occurs depending upon the presence of leading-edge separation. The mathematical formulation was primarily based upon test flow visualization (Refs. 2, 3, 7 and 8) at high airfoil incidence where separated flow exists as sketched in Figure 5 (inset view for stalled/Helmholtz flow) or in Figure 8. However, at low incidence, leading-edge separation is either non-existent or too insignificant to sustain a vortex. As discussed in Section 5.3 (and visualized in Figures 30 and 31) of Volume I to this report, even at low angle of attack the high cross-flow shear layer above the jet propagates vorticity which causes the jet region to develop a high swirl rate as it is swept aft over the wing. Note that the analysis is limited to wing root blowing cases.

4.1.1 Cross-Flow Jet and Vortex Trajectories

The mean trajectories of the jet and vortex (center of swirl) were estimated from the flow visualization photographs cited previously and plotted in Figure 13. The corresponding jet and vortex paths, as approximated in Appendix A, are shown in the figure to be in very good agreement with the test data as interpreted for $C_\mu \simeq .4$ and $\alpha = 8.5$ degrees. Surprisingly, the simplified vorticity integration performed herein predicts that the mean path of concentrated vorticity crosses over and aft of the jet apparent trajectory for an angle of attack below that for natural airfoil stall. The analysis makes the arbitrary assumption that the vortical layer extends aft from the wing apex, or the junction of the wing leading-edge and fuselage sidewall. This is not apparent in the test results except, perhaps, at high

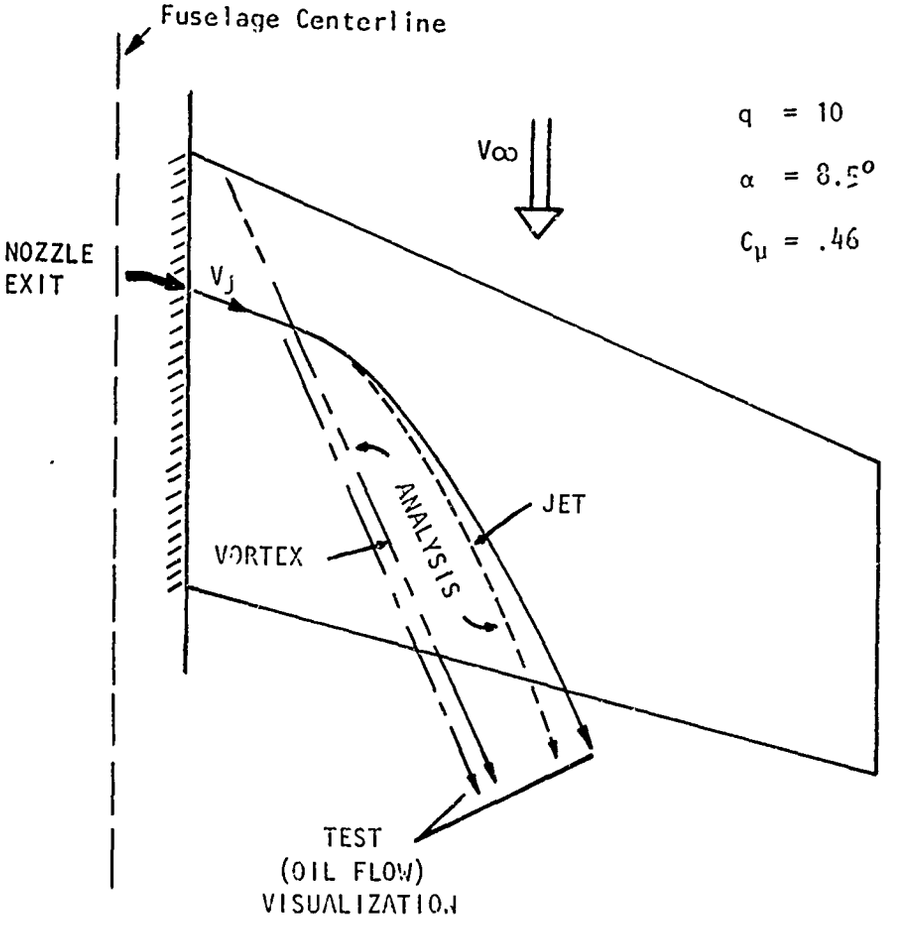

FIGURE 13 COMPARISON OF THEORETICAL AND EXPERIMENTAL VORTEX AND JET CENTERLINE TRAJECTORIES AT α = 8.5 DEGREES

angles of attack (c.f. Volume I, Figure 27).

4.1.2 Differential Pressures

At low incidence, the accuracy of the basic vortex-lattice (V-L) program is examined in Figure 14(a). At $C_\mu = 0$ and $\alpha = 8.5$ degrees, the flow is naturally attached and, as anticipated, the differential pressures from Volume I measurements agree quite well with the analysis. The leading-edge singularity is characteristic of all lifting surface theories. Although approximate corrections could be made for the finite-radius leading-edge of the wing and for the minor thickness or camber effect observed at about mid-chord position in the tests, this was not deemed to be of sufficient importance for the objective of predicting power-augmented lift effects.

For a spanwise blowing momentum coefficient, $C_\mu = 0.46$, the comparison of chordwise differential pressure variations at 36.4 percent of span, as in Figure 14(b), indicates that the theoretical simulation generally predicts lift increment trends like those measured in the wind tunnel tests. The effective thickness/camber increase over the aft chord region, under the jet/vortex path, is similar in distributed form to that from the tests, but is slightly deficient in C_p magnitude and locations of pressure peaks. Some of this may be due to the relatively coarse spanwise grid spacing (5 spanwise and 10 chordwise collocation stations) used in the lattice (V-L) program to minimize computer time. In the case of highly curved trajectories, the jet and vortex induced velocities were diagonally distributed over a wing collocation panel, in close proximity to lattice singular points. A smoothing process described in Section 3.5 minimized the possible errors caused by such a "lumped-parameter" system, but some biased weighting is

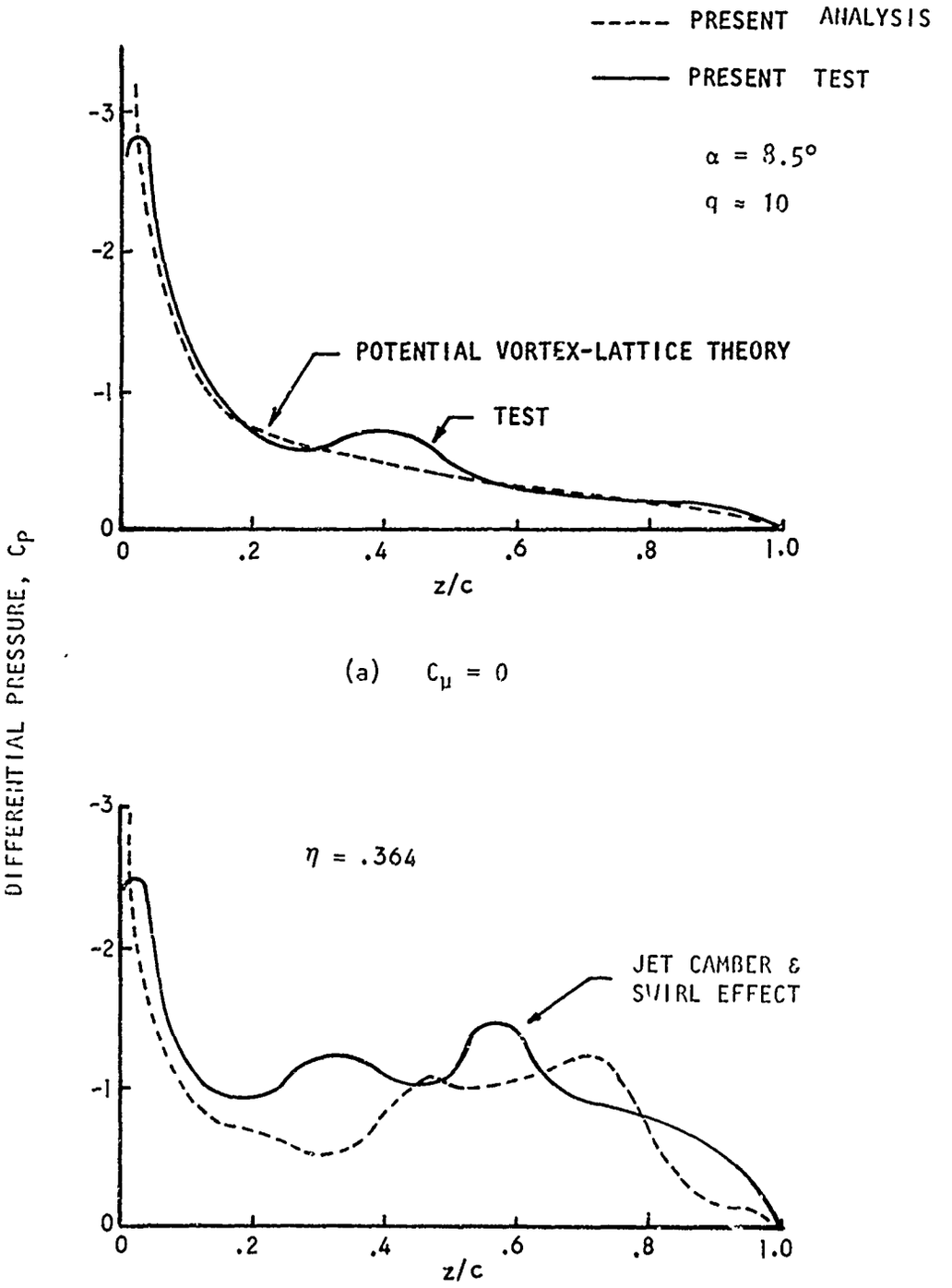

FIGURE 14 COMPARISON OF THEORY AND EXPERIMENT AT LOW ATTITUDE WHERE A LEADING EDGE VORTEX IS NOT FORMED

inevitable in the correction formulas employed. It is more likely that the approximations in vortex strength and jet displacement thickness cause the major discrepancies observed in this non-optimum case. In the optimum lift augmentation cases, with a highly separated flow region and less effective cross-flow velocity, the error in calculated jet displacement thickness is probably less significant to the overall lift predictions.

4.2.0 HIGH INCIDENCE RESULTS OF VORTEX-LIFT CONTROL THEORY

Leading-edge or primary vortex-lift augmentation is shown in Volume I to be effective in increasing maximum lift for attitudes above normal stall and for wing root blowing momentum coefficients greater than about 0.1. Lesser amounts of C_μ do, of course, provide lift augmentation by other means, as discussed in Section 4.1.0. A high C_μ value of 0.46, above the optimum, was selected for most of the analytical studies since it was desired to emphasize the strong vortex formation and control mechanisms.

4.2.1 Cross-flow Jet and Vortex Trajectories

The experimental jet and vortex trajectories are presented in Figure 15, as interpreted from oil flow photographs in Figure 30 of Volume I at a slightly lower value of C_μ. The analytical approximation for reducing the effective cross-flow velocities, V_{e_i}, across the span yields very good agreement with the test observations for both vortex and jet paths. The jet effective spread angle, $\gamma = 30$ degrees used in the analysis is not directly determinable from the surface flow pictures. But, as pointed out in Volume I, if the jet direction and spread rate is not proper, the vortex will not be positioned properly behind the wing leading-edge. For the oval nozzle used in these

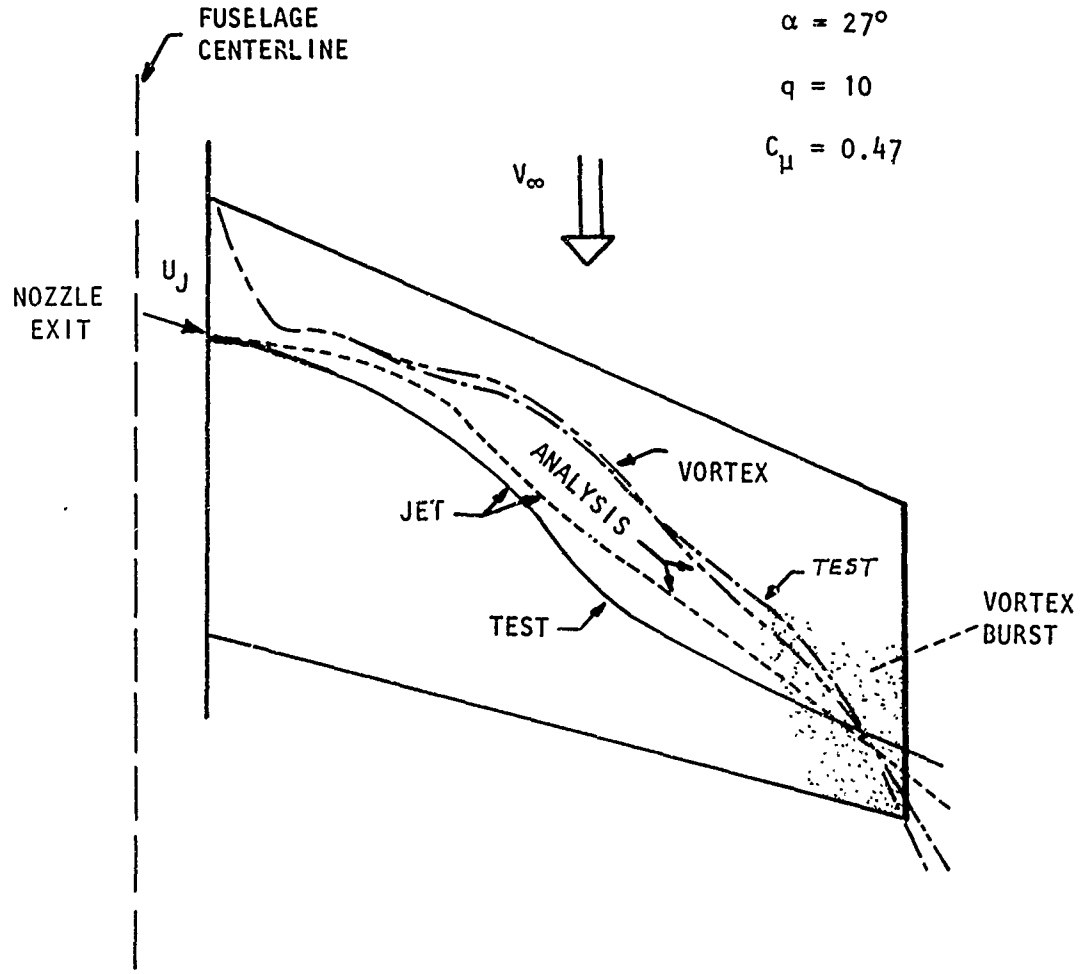

FIGURE 15 COMPARISON OF THEORETICAL AND EXPERIMENTAL VORTEX AND JET CENTERLINE TRAJECTORIES AT α = 27 DEGREES

tests (see Volume I), the geometric exit angle of 12 degrees aft relative to the wing leading-edge sweep angle was not the observed initial jet trajectory angle, θ_o, in the photographs. Further study is needed on the effects of nozzle wall and orifice unsymmetries. For this analysis, the initial angle was adjusted to match that in the photographs in order to ensure reasonable starting conditions. Fortunately, no other adjustments in coefficients for the semi-empirical trajectory solutions presented in Appendix A were required to achieve the good agreement in Figures 13 and 15 for vortex location versus span over the range $8.5° < \alpha < 27°$ and $0.1 < C_\mu < 0.46$.

4.2.2.0 Stall/Burst/Reynolds Number Effects

Vortex burst was predicted, accompanied by a rapid increase in apparent vortex radius, at about 80 percent of span, using the Rossby number criteria (Appendix A). The oil streak lines in Figure 30 of Volume I also show a sudden divergence in this outer span region. Simultaneously, the pitching moment for similar C_μ and angle of attack (27°) in Figure 29 of Volume I shows a sudden reversal in trend, toward nose-up conditions. Thus the tests indicate the possibility of partial wing-tip stall initiated by vortex burst.

This same case was later rerun with a factor of twelve increase in wing-scale, and the Rossby number did not predict vortex burst. Yet the differential pressures, prior to modification for burst/separated flow at small-scale, as described in Section 3.5.3, showed only minor changes with scale. Professor Owen's dissipation analysis employed herein (Appendix A) does predict changes with scale in the vortex ageing process. This predicted improvement in spanwise blowing at large scale is partially substantiated by larger scale

model tests discussed in Section 5.2.1, Volume I, since slightly less momentum coefficient seems to be required for a given lift increment. Unfortunately, some differences in configuration existed in these Lockheed-funded tests, so no firm conclusions can be drawn.

Some discussion of the effects of the natural stall angle for a given airfoil (in this case, 14 degrees), on the two- and three-dimensional analyses has already been given in Sections 2.2 and 3.5. Also, the starting-vortex strength limitations of Figures 5-7 must be kept in mind. Then the vortex-lift, ΔC_{L_v}, variations with angle of attack for two extremes of C_μ (0.115 and 0.46) can be calculated from the 3-D simulations, presented as dashed lines in Figure 16. The "unstalled" limit angle is again shown; but, in addition, the vortex-burst initiated, partial wing stall region is approximately indicated. This effect occurs at high incidence where the C_μ is only marginally sufficient to entrain fluid and propagate fully through the leading-edge separation region, causing local chordwise reattachment. The test points in Figure 16 at similar C_μ's (0.155 and 0.46) show the tendency, as hypothesized in the analysis, to reach an asymptotic ΔC_{L_v} limit as this burst/stall condition is approached. At lower angles of attack, the differences relative to theory are a result of the difficulties in separating out, from the test data, the lift increment due to the vortex alone, as estimated for Figure 32 in Volume I of this report. This problem is even more complex when combined inboard and outboard spanwise-blowing jets are used.

4.2.2.1 Lift Increments and Causes - The total lift from potential, vortex lattice theory (Refs. 22-24) compares well with the test data prior to stall,

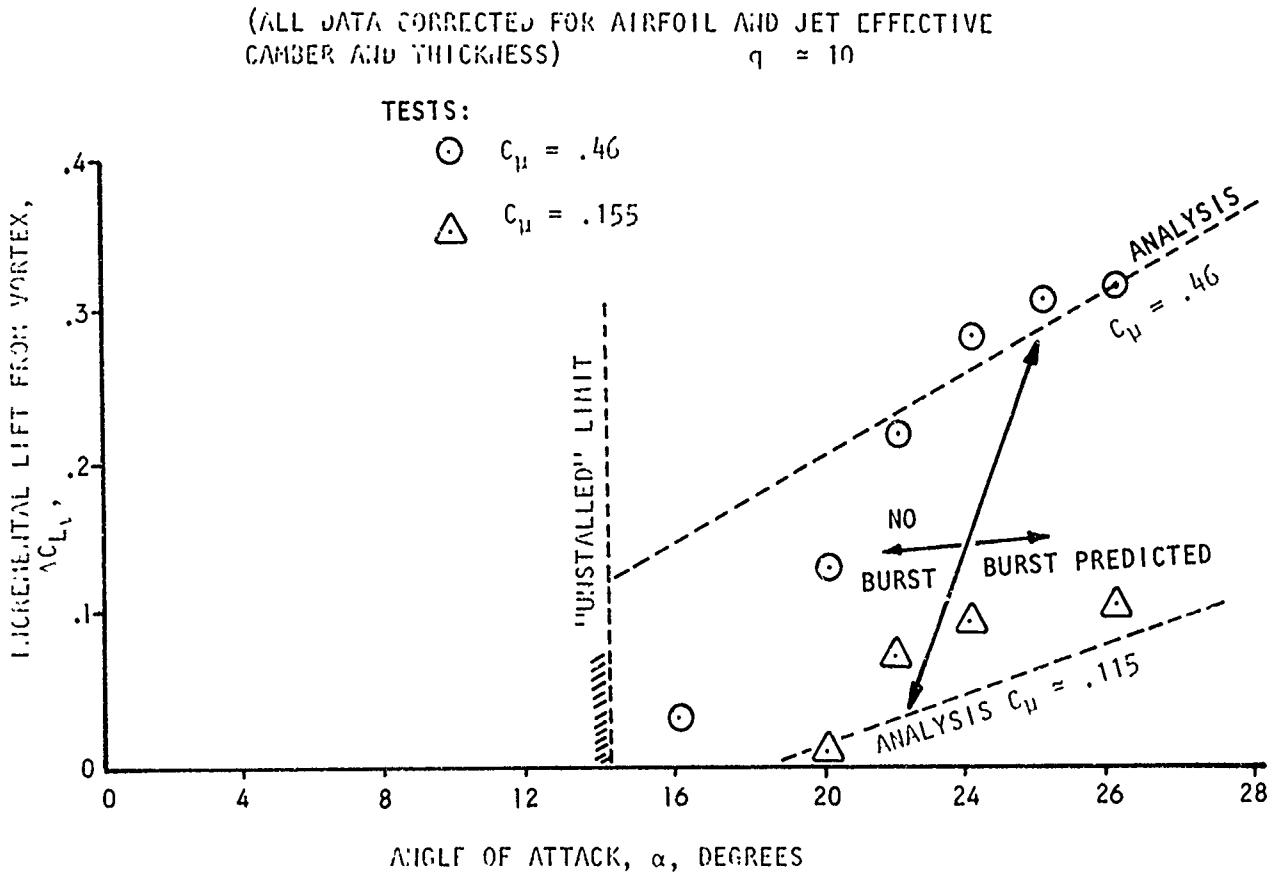

FIGURE 16 COMPARISON OF BOTH LOW- AND HIGH-INCIDENCE STALL FOR ΔC_{L_v} IN TESTS WITH CORRESPONDING EFFECTS FROM THE ANALYSIS

as shown in Figure 17(a) at $C_\mu = 0$. This does imply compensating effects, concerning the natural wing camber and thickness corrections for this Lockheed super-critical airfoil, for middle range α's, since the V-L method does not include these. A non-planar wake is considered, however, giving some nonlinear induction in the lift.

Obviously, any powered-lift technique which reattaches the flow at above-stall angles will yield significant ΔC_L increments, shown as "Indirect Augmentation" in Figure 17(b). This probably consists largely of a boundary layer control effect related to the spanwise blowing jet spreading over the upper surface aft of the reattachment zone. Essentially, this re-establishes the potential flow character, with the addition of some effective camber due to the jet displacement thickness, shown by the dotted line in Figure 17(b). Refer to the upward, nearly parallel shifts in the C_L versus α curves, at zero incidence, in Figure 29 of Volume I.

The increase in the slope of the lift curve above the stall is directly attributed to the vortex and its induction effects through the elements of the feeding sheet (dashed line in Figure 17(b)). Actually, most of the lift above the mean stall level exists due to the reattachment caused by the formation of at least a small vortex near the leading-edge, so the above is an arbitrary division of augmentation increments due to the vortex.

At very high angles of attack, the vortex-burst-created stall over part of the span causes some lift loss (dot-dashed line, Figure 17(b)), and this agrees quite well with the test stall character above $\alpha = 25$ degrees (solid line in the figure).

(a) $C_\mu = 0$

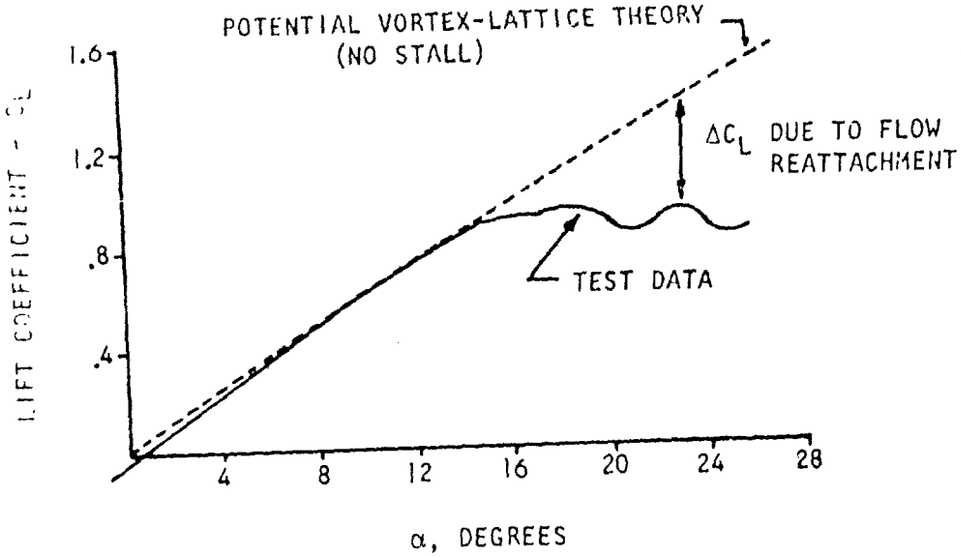

(b) C_μ=.46 ; KEY:

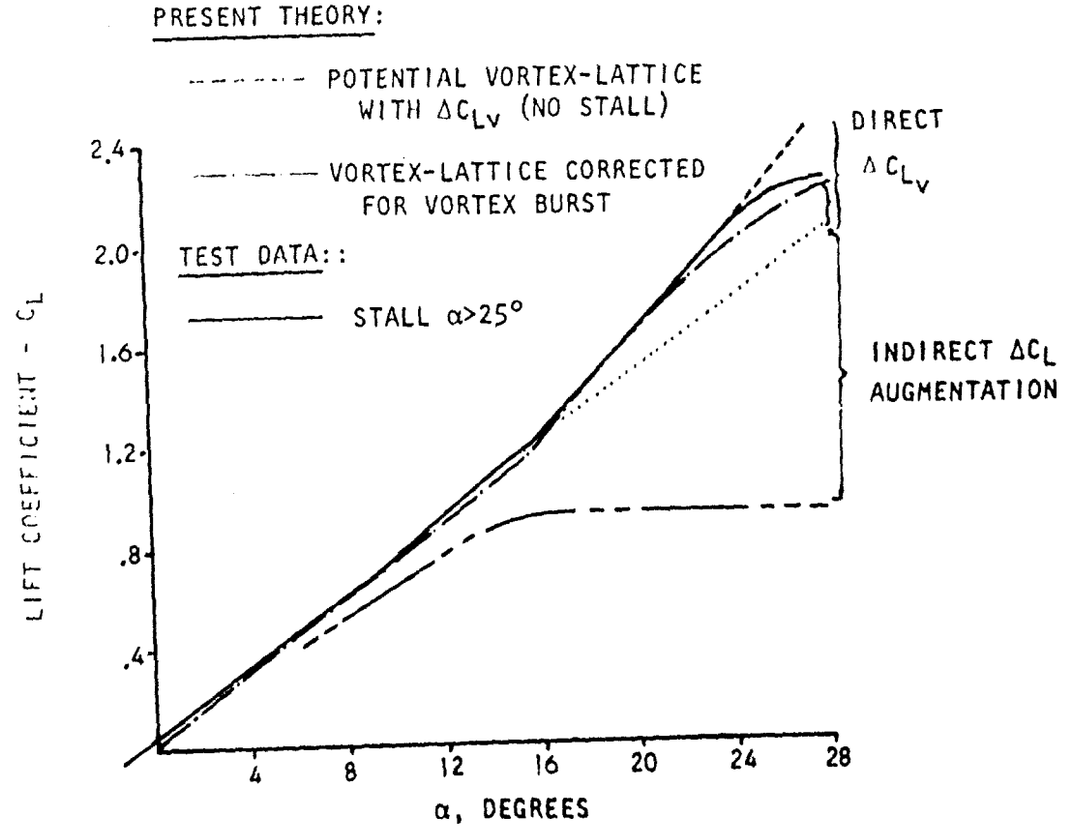

FIGURE 17 COMPARISON OF INCREMENTS OF LIFT FROM VORTEX-LIFT AUGMENTATION AND SPANWISE BLOWING IN BOTH TESTS AND ANALYSES

4.2.2.2. Differential Pressures - The previously discussed wing tip stall phenomenon is revealed in part by the non-potential flow character of the aft-chord C_p distribution, at 91 percent of semi-span, shown in the top part of Figure 18. The nearly flat aft distribution is more like that for Helmholtz flow, used to modify the V-L simulation for wing regions encompassing the indication of vortex burst (See Section 3.5.3).

At 72.7 percent of semi-span, the aft-chord differential pressures are again in agreement between test and theory. There is some indication that the simulation under-predicts the leading-edge vortex strength at this station; but, unfortunately, at critical chordwise stations the pressure measurements were consistently unreliable, as indicated in the figure.

At 36.4 percent of semi-span, the vortex induced peak is predicted quite accurately; and these C_p's probably would improve if the wing leading-edge singularity, from the V-L method, were corrected for a finite leading-edge radius. Other minor differences may also improve if a greater number of collocation panels are selected, as discussed relative to Figure 14 (Section 4.1).

Similar agreement between test and analysis is shown in Figure 19 for an intermediate angle of attack, $\alpha = 21$ degrees, and $C_\mu = 0.44$. At this outboard span station the simulation seems to over-predict the jet-cross-flow super velocity effect over aft chord sections, and a smoother transition between the vortex and jet-swirl pressure peaks is indicated than that measured in the wind tunnel model tests.

The pressure distributions in Figures 14 and 18 reveal some interesting features of the flow over the upper surface of the wing. For spanwise blowing at low wing incidence, the aft-chord jet swirl peak is very apparent. But,

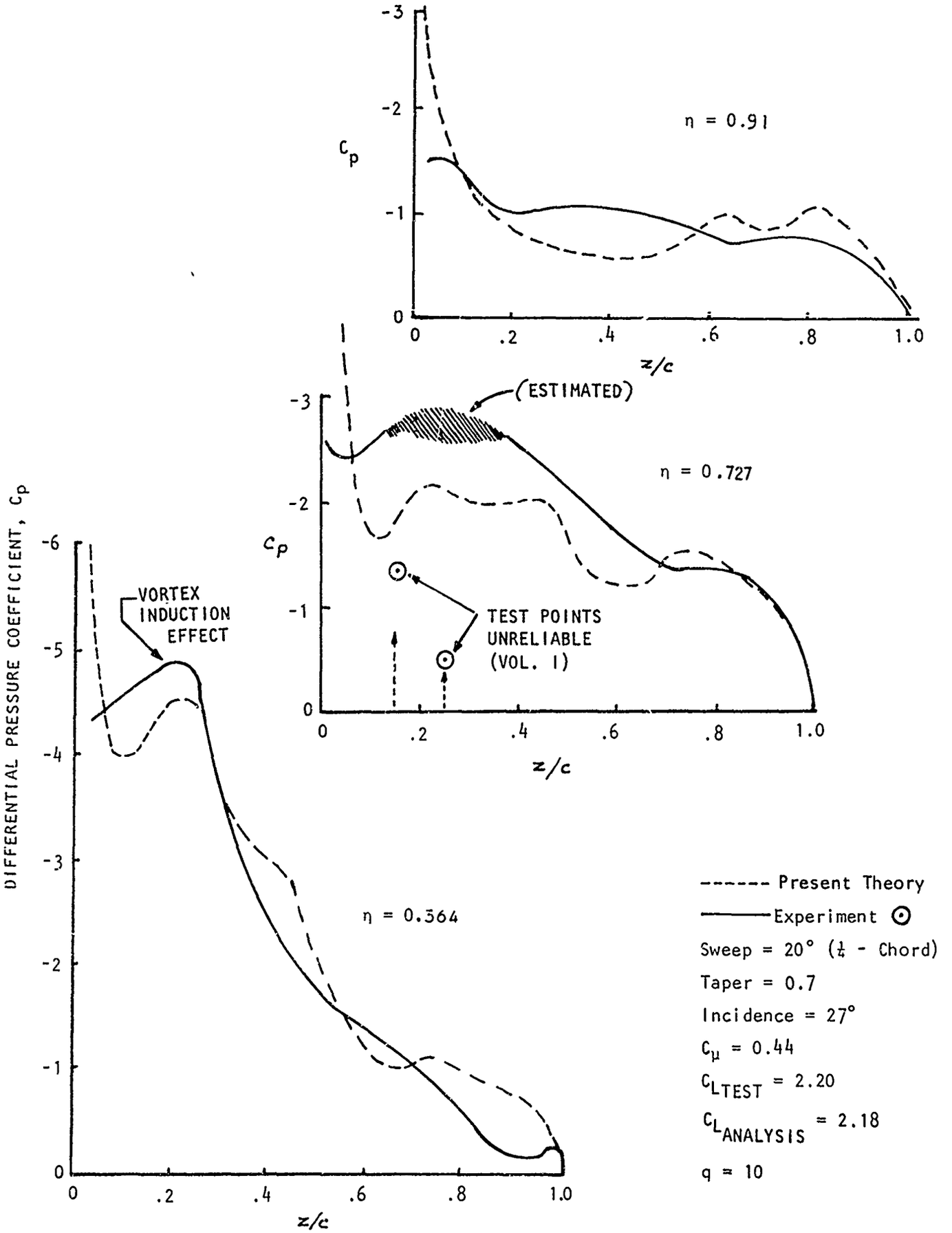

FIGURE 18 COMPARISON OF CHORDWISE PRESSURE DISTRIBUTION FOR THEORY AND EXPERIMENT WITH SPANWISE BLOWING OVER A SWEPT WING

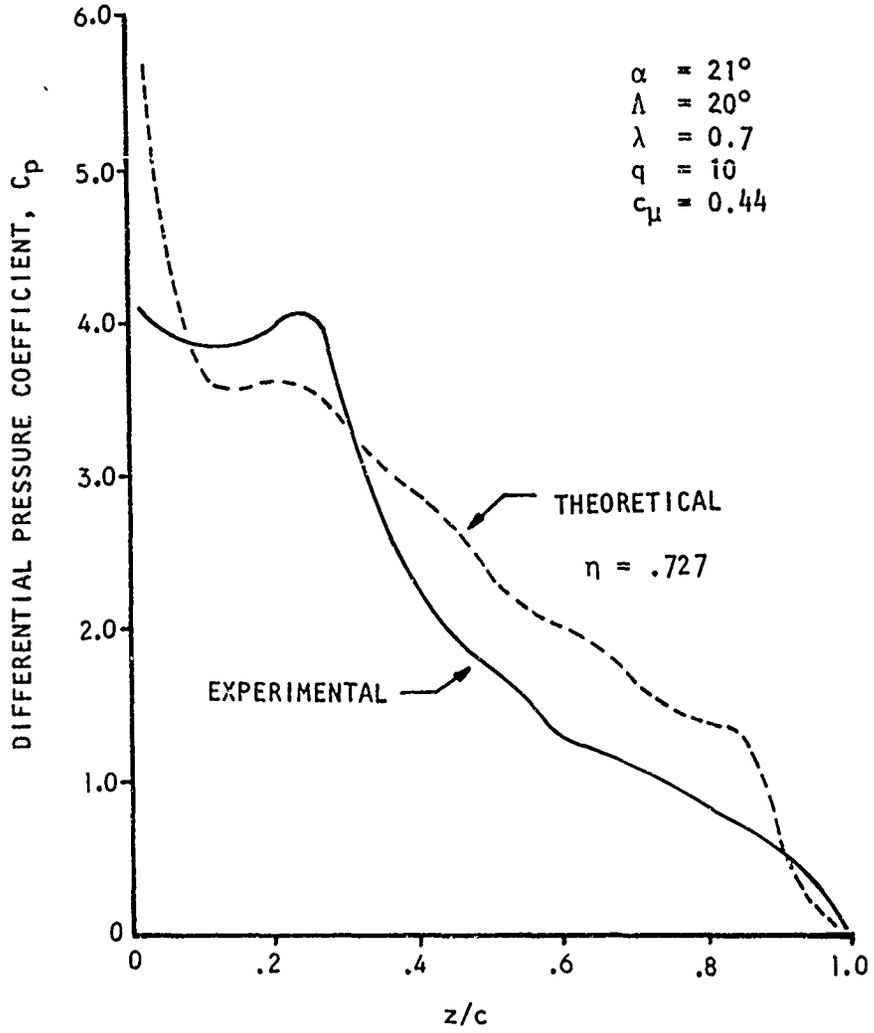

FIGURE 19 COMPARISON OF CHORDWISE PRESSURE DISTRIBUTION FOR THEORY AND EXPERIMENT WITH SPANWISE BLOWING OVER A SWEPT WING

at high attitudes, the influence on the pressure coefficient caused by the vortex and feeding sheet near the leading-edge is much more dominant. The increased suction is partly attributable to the higher upwash velocities forward of and at the vortex center within the "cavity" or decelerated mean flow region. As the reattachment point is approached, aft of the vortex for the most inboard station shown in Figure 18, the pressure increases rapidly due to downwash velocity components from both the vortex and jet impingement on the surface forward of the nozzle. However, the jet wake provides a cross-flowing super-velocity to elements of the upper surface vorticity feeding sheet which then causes another, smaller, suction peak to form farther aft on the chord. These effects are less pronounced, but are still apparent at more outboard stations. The finite displacement thickness of the jet suggests a local camber effect; but the ΔC_p's are higher than could be expected purely by this mechanism.

The three-dimensional simulation uses a feeding sheet with vortex elements which can allow the jet to produce pressure variations qualitatively consistent with the above experimental observations. Since quantitative agreement of the modeling technique with Polhamus' leading-edge suction analogy for delta wings (Refs. 20 and 21) has been shown (Figure 10), future research would be desirable to determine if some combination of these methodologies could be used to predict the pressure distributions (and pitching moments) qualitatively for more general planforms either with or without powered lift effects.

4.3.0 SPANWISE LIFT DISTRIBUTIONS AND TOTAL LIFT

The changes in spanwise lift distribution caused by vortex-lift augmentation are apparent in Figure 20. The potential (V-L) theory at high incidence, $\alpha = 27°$, arbitrarily assumes attached flow to give a classical, near-

elliptic distribution. As normalized to the Maximum C_L in each case, and using a blowing momentum coefficient, $C_\mu = 0.46$, the outboard lift drops relative to that at inboard sections. Part of this is due to wing-tip stall, as previously discussed. But the calculated inboard $C_\ell \frac{c}{\bar{c}}$ peak is partly due to the vortex augmentation and partly due to thrust recovery. For example, an integration of the test pressure data at 36.4 percent of semi-span yields only the normal force coefficient $C_N \frac{c}{\bar{c}}$, and the inboard hump is not apparent in this value. The leading-edge thrust and the drag at that wing station are difficult to obtain because of the few pressure taps available. Thus a rough calculation was made for the lift-vector components of thrust and drag from the theory, and then combined with the vertical-component of test normal force at $\alpha = 27°$. This estimated test point is shown in Figure 20 as a dotted circle. Relatively good agreement between test and analysis is then indicated. However, the fuselage correction in the simulation is very approximate (See Section 3.5.3), so the most inboard part of the curve should not be used quantitatively. Intuitively, a decline of $C_\ell \frac{c}{\bar{c}}$ in this region would be expected at these high angles of attack.

Comparison of test and analysis for $C_{L_{MAX}}$ versus C_μ in Figure 21 shows very good agreement. Empirical adjustments to the two-dimensional starting conditionsshould be recalled, however, so as to not give misleading conclusions on the state-of-the-art in this vortex-lift augmentation theory. Also, it is fortunate that the classical camber and thickness corrections apply so well to these test conditions. For other model configurations, the modified vortex-lattice program (Figure 11) has no basic limitations. But a more analytical formulation of the cross-flowing jet and viscous/boundary-layer affects is still necessary for more general applications.

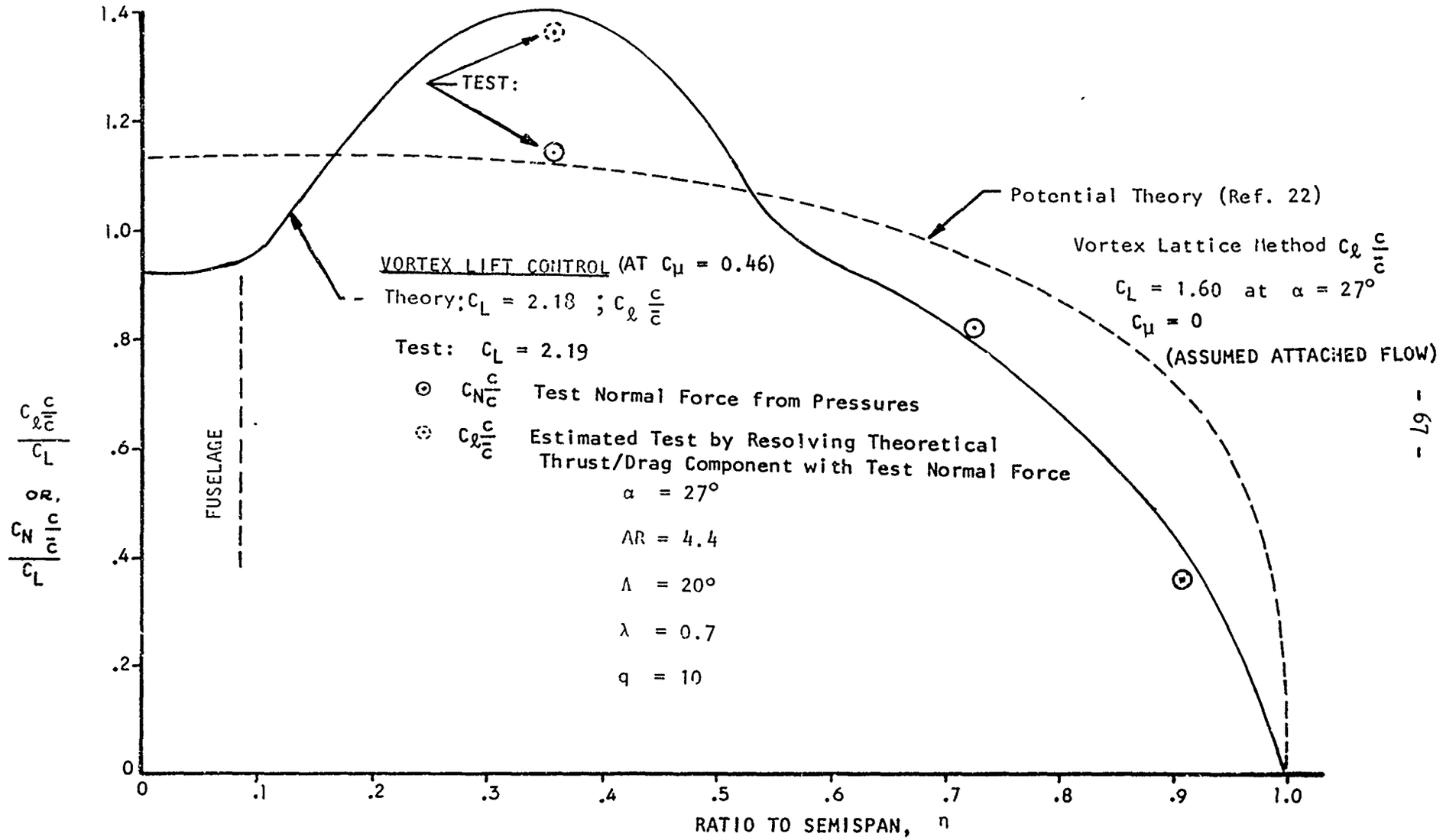

FIGURE 20 COMPARISON OF LIFT DISTRIBUTION FROM PRESENT THEORY AND TESTS FOR C_μ = .46 WITH THAT FROM POTENTIAL THEORY AT C_μ = 0

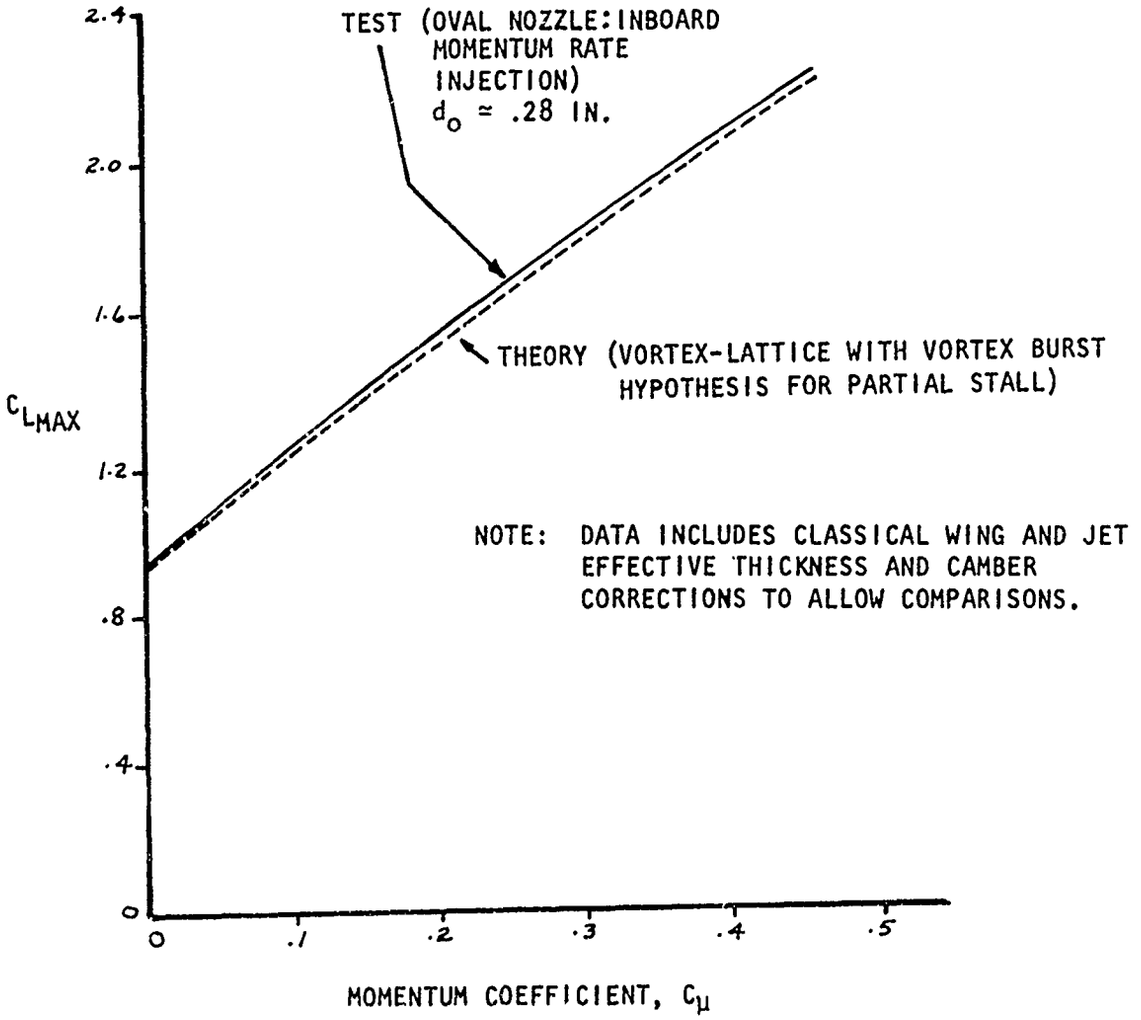

FIGURE 21 EFFECT OF SPANWISE BLOWING JET ON $C_{L_{MAX}}$

5.0 CONCLUSIONS AND RECOMMENDATIONS

5.1 CONCLUDING REMARKS

The three-dimensional analysis for vortex-lift control, presented herein, is admittedly very empirical in nature. However, the presence of each of the hypothesized elements of the phenomena inherent in spanwise blowing is strongly indicated by the experimental evidence delineated in Volume I of this report.

A previous analytical solution for viscous vortex flows, verified by idealized experiments, also has been presented in revised form so as to show characteristic dependence on radial-inflow Reynolds Number and Rossby-number concepts. This describes a fundamental physical mechanism for causing an organized vortex to grow from an upstream, separated shear-layer and to be stabilized. In addition, if a separated flow region exists or can be created adjacent to this feeding sheet, then adverse pressure gradients may prevent any major (periodic or steady) streamwise shedding from a predominantly-spanwise vortex. Such adverse pressures may be created, for instance, by a spanwise jet just downstream of the vortex formation region. Over a wing upper surface, this results in a strongly sheared three-dimensional wall-jet velocity profile. An appropriate Stokes' integration of this wall-jet vorticity, in planes oriented so as to yield increased circulation to the primary vortex, provides the correct amount of vortex-lift augmentation in comparison with experimental data. The ensuing viscous dissipation, calculated using a realistic and time-dependent turbulent eddy viscosity, does not significantly reduce this lift augmentation at high angles of attack.

The prediction method for vortex-lift augmentation derived herein requires initially a two-dimensional source-sink/vortex model for locating the leading-edge vortex. In addition, a first estimate is made for this vortex circulation strength consistent with the appropriate boundary conditions and momentum coefficients. Then, with available, approximate cross-flowing-jet solutions for trajectory and entrainment, the spanwise distribution of the equivalent two-dimensional singularities are estimated. These induction effects are combined with those from a spatially varying, finite-element vortex feeding sheet emanating from the wing leading edge. Subsequently, the combined supervelocities are employed in a vortex-lattice solution for general wing configurations. The total forces and aerodynamic coefficients are compared with the corresponding test data from Volume I, and relatively good agreement is obtained. Optimum mass-momentum injection conditions can be predicted using this method, for initial design estimates. Favorable Reynolds Number effects are also possible since a large scale model showed less tendency for the augmented vortex to burst, and corresponding flow separation over sections of the wing is less likely to occur. Otherwise, lift coefficients predicted for small scale models are substantially the same as those for large scale models, similar to the conclusions from scaled tests in Volume I of this report.

The combination of nonlinear viscid and inviscid mathematical elements used in this initial formulation require that an iterative and semi-empirical procedure be employed for solution. Now that the heuristic objectives of this research program have been satisfied (i.e., to obtain an improved physical understanding of the numerous flow mechanisms in spanwise-blowing/vortex lift augmentation), more sophisticated viscous flow theories are required to

reduce the degree of empiricism and thereby to enable application of the above methods more widely and with greater confidence.

5.2 RECOMMENDATIONS

The following tasks are recommended for future research to advance current understanding of the spanwise-blowing phenomenon:

1. Develop a rational analysis of jet flow in a cross-stream with a parallel wall. This should involve both mathematical and experimental investigation of jet structure, to incorporate measured turbulence parameters in an analytical framework for predicting jet spread rate and decay using three-dimensional boundary layer methodology.

2. Further refinement of the two-dimensional theory, incorporating a leading-edge feeding sheet for the vortex and inclusion of rigorous criteria for selecting vortex position uniquely for each flow condition.

3. Basic research is needed on the phenomenon of vortex bursting, especially in the presence of a lifting surface.

4. Finally, the results of items (1) - (3) should be used to refine the present vortex-lattice scheme for three-dimensional loads to the point that optimum design studies can be made.

REFERENCES

1. Theisen, J. G., "Vortex Periodicity in Wakes," AIAA Paper 67-34, AIAA 5th Aerospace Sciences Meeting, New York, N. Y., January 23-26, 1967.

2. Cornish, J. J. III, "High Lift Applications of Spanwise Blowing," ICAS Paper No. 70-09, the 7th Congress of the International Council of the Aeronautical Sciences, ROMA, Italy, Sept. 14-18, 1970.

3. Dixon, C. J., "Lift Augmentation by Lateral Blowing over a Lifting Surface," AIAA Paper No. 69-193; Presented at the AIAA/AHS VTOL Research, Design and Operations Meeting, Georgia Institute of Technology, Atlanta, Georgia, February 17-19, 1969.

4. Scruggs, R. M. and Marris, A. W., "An Experimental and Analytical Study of Vortex Blocking," Lockheed-Georgia Research Memorandum, ER-9671, December, 1967. (Requests for this document should be submitted directly to the Lockheed-Georgia Co.)

5. Theisen, J. G., "Vortex Flows in Wakes," Proceedings, Boundary Layer Symposium, Lockheed-Georgia Research Laboratory, ER-8290, September 3, 1965. (Requests for this document should be submitted directly to the Lockheed-Georgia Co.)

6. Scruggs, R. M., "An Investigation of Near Wake Effects in Airfoil Dynamic Stall," Ph.D. Thesis, Georgia Institute of Technology, GITAER Report 71-1, March 1971.

7. Dixon, C. J., "Analysis of Experimental Force Data for Lift Augmentation by Spanwise Blowing Over Trailing Edge Flaps and Aircraft Control Surfaces," prepared under Contract to Naval Air Systems Command, Lockheed-Georgia Company, Engineering Report ER-11190, September 30, 1971.

8. Dixon, C. J., "Lift and Control Augmentation by Spanwise Blowing over Trailing Edge Flaps and Control Surfaces," AIAA Paper No. 72-781, Los Angeles, California, August 7-9, 1972.

9. Milne-Thomson, L. M., Theoretical Hydrodynamics, The Macmillan Company, 2nd Ed., 1950.

10. Tyler, E., "Vortex Formation Behind Obstacles of Various Sections," Philosophical Magazine, Series 7, Vol. II, No. 72, April, 1931.

11. Fage, A., and Johnson, F. C., "The Structure of Vortex Sheets," R&M No. 1143, British ARC, 1927.

12. Cornish, J. J., and Scruggs, R. M., "A Synthesis of the Lift and Drag Characteristics of a Flat Plate," Lockheed-Georgia Research Memorandum ER-9419, June 1968. (Requests for this document should be submitted directly to the Lockheed-Georgia Co.)

13. Leibovich, S., "Wave Motion and Vortex Breakdown," AIAA Paper No. 69-645, San Francisco, June 16, 1969.

14. Owen, P. R., "The Decay of a Turbulent Trailing Vortex," The Aeronautical Quarterly, February, 1970.

15. Hackett, J. E., and Miller, H. R., "A Theoretical Investigation of a Circular Lifting Jet in a Cross-Flowing Mainstream," AFFDL-TR-70-170, January, 1971.

16. McAllister, J. D., "A Momentum Theory for the Effects of Cross Flow on Incompressible Turbulent Jets," Ph.D. Thesis, U. of Tennessee, August, 1968.

17. Newman, B. G., "The Prediction of Turbulent Jets and Wall Jets," Canadian Aeronautics and Space Journal, October, 1969.

18. Margason, Richard, J., "The Path of a Jet Directed at Large Angles to a Subsonic Free Stream," NASA TN D-4919, November 1968.

19. Brown, C. E., and Michael, W. H., "Effect of Leading Edge Separation on the Lift of a Delta Wing," Journal of Aeronautical Sciences, October, 1954.

20. Polhamus, E. C., "A Concept of the Vortex Lift of Sharp Edge Delta Wings Based on a Leading Edge Suction Analogy," NASA TN D-3767, December 1967.

21. Polhamus, E. C., "Predictions of Vortex-Lift Characteristics Based on a Leading Edge Suction Analogy," AIAA Paper No. 69-1133, October 20-24, 1969.

22. Hackett, J. E., and Evans, M. R., "Vortex Wakes Behind High-Lift Wings," Journal of Aircraft, Col. 8, No. 5, May 1971, pp 334-340 (also, see AIAA Paper 69-740, 1969).

23. Hackett, J. E., and Holmes, A. E., "Vortex Roll-Up Behind High-Lift Wings, Calculation of Velocities Due to Three-Dimensional Arrays of Vortices," Lockheed-Georgia Research Memorandum ER-10406-4, January 1970. (Requests for this document should be submitted directly to the Lockheed-Georgia Company.)

24. Hackett, J. E., and Praytor, E. B., "Vortex Roll-up Behind High-Lift Wings, Three-Dimensional Vortex Collocation Program," Lockheed-Georgia Research Memorandum ER-10406-2, June 1970 (Also, Lyman, V. "Description and Utilization of the Vortex Collocation Program (VLWINGD2);" LG-73-ER-0164, September 1973. (Requests for this document should be submitted directly to the Lockheed-Georgia Co.)

25. Hackett, J. E., and Theisen, J. G., "Vortex Wake Development and Aircraft Dynamics", Proceedings, AFOSR/BSRL Symposium on Aircraft Wake Turbulence, September 3, 1970.

26. Abramovich, G. N., The Turbulent Theory of Jets, The MIT Press, Cambridge, Mass., 1963 (p. 491).

27. Brady, W. G., "Numerical Analysis of Two Free-Boundary Problems in Fluid Mechanics", AIAA Paper No. 67-217, Jan. 23-26, 1967.

28. Ruo, S. Y., Yates, E. C., Jr., and Theisen, J. G., "Calculation of Unsteady Transonic Aerodynamics for Oscillating Wings with Thickness", AIAA Paper No. 73-316, March 19-20, 1973.

29. Bramble, J. H., Numerical Solution of Partial Differential Equations, Academic Press, Inc., New York and London, 1966. (pp. 369-373).

30. Singleton, R. E., Nash, J. F., Carr, L. W. and Patel, V. C., "Unsteady Turbulent Boundary-Layer Analysis", NASA TM X-62, 242, February 1973.

31. Jacobs, W. F., "Berechnung des Schiebe-Roll momentes fur Flugel-Rumpfanordnungen", Jahrbuch 1941 der deutschen Luftfahrtforschung, 1941.

32. Theisen, J. G., "V/STOL Stability and Control in Turbulence", AIAA/AMS Paper, Proceedings, Third National Conference on Aerospace Meteorology, New Orleans, La., May 6-9, 1968.

33. Theisen, J. G., and Haas, J., "Turbulence Upset and Other Studies on Jet Transports", Journal of Aircraft, Vol. 5, No. 4, July - August, 1968.

34. Long, R. R., "Velocity Concentrations in Stratified Fluids", Journal of the Hydraulics Division, Proceedings of the ASCE, (pp. 9-26), January, 1962.

35. Lezius, P. K., "Study of the Far Wake Vortex Field Generated by a Rectangular Airfoil in a Water Tank", AIAA Paper No. 73-682, July, 1973.

36. Nash, J. F., "Some Calculations Extending the Williams' Model of the Decay of Trailing Vortices", Lockheed-Georgia Company Engineering Report LG73ER0191, October, 1973. (Requests for this document should be submitted directly to the Lockheed-Georgia Company.)

37. Schlichting, H., Boundary Layer Theory, p. 605, 4th edition, McGraw-Hill, 1960.

38. Rayleigh, Lord, "On the Dynamics of Revolving Fluids", Scientific Papers, Vol. 6, Cambridge Univ. Press, 1916, p. 447-453.

39. Korner, H., "Verechnung der potential Theoretischen Stromung um Flugel-Rumpf-Kombinationen und Vergleich mit Messungen", Zeitschrift Fur Flugwissenschaften, Vol. 20, p. 356, September 1972.

40. Long, R. R., "Sources and Sinks at the Axis of a Rotating Fluid", Quarterly Journal of Mechanical and Applied Mathematics, Vol. 9, p. 385, 1956a.

41. Lambourne, N. C., and Bryer, D. W., "The Bursting of Leading-Edge Vortices--Some Observations and Discussion of the Phenomenon", ARC R&M No. 3282, 1962.

42. Hall, M. G., "A New Approach to Vortex Breakdowns", Proceedings 1967 Heat Transfer and Fluid Mechanics Institute, p. 319, Stanford U. Press, 1967. (See also, "The Structure of Concentrated Vortex Cores," Progress in Aeronautical Sciences, Vol. 7, Edit. by D. Kucheman, Pergamon Press, N. Y., p. 53-110, 1966.)

43. Smiley, R. F., "Experimental Investigation of Wake Velocity Fluctuations Behind Stalled Wings at Reynolds Numbers Up to 4.8 Million", Allied Research Associates, Inc., Report 9G87-F, Final Report of NASC Contract No. N00019-71-C-0360, (Available as AD-763468) Feb. 1973.

APPENDICES

APPENDIX A: Summary of Approximate Jet/Vortex Viscous Flow Methods.

The physical problem discussed in this report poses so many complex flow interactions that theoretical analyses of even sub-elements of the formulation (as outlined in Figure 11 of Section 3.0) have only been accomplished in part, or semi-empirically. The purpose of this Appendix is to summarize approximations obtained from available literature and employed with minor modifications elsewhere in the text.

General Formulas for Jets and Vortices

The free-jet in a cross flow is still usually treated semi-empirically, although numerical or finite-element methods (e.g., Refs. 15 and 18) are recently much improved. Unfortunately, these methods are cumbersome and lacking in consideration of the boundary-layer, viscous wall-jet interaction most essential to this problem. On this basis, the momentum entrainment theory developed by McAllister (Ref. 16) seems most appropriate, yet simple in form. Using the momentum theorem and specific mass-momentum flux data, he showed that the entrained mass flux, Q, carries the undisturbed cross-flow velocity, V_∞ into the jet in such a way that it adds the momentum, QV_∞, to the jet flow. A principal modification employed herein is the replacement of V_∞ by V_e, the effective cross-flow velocity (Equation 21 in Section 3.5), defined as

$$V_e \cong V_\infty \cos(\theta_o + \Lambda) - e_o V_{\theta_o} \qquad (A.1)$$

where

θ_o is the initial jet trajectory angle, as shown in Figure A.1,

V_{θ_o} is the initial tangential velocity of the first unbound (leading-edge) vortex element, at a height, $(y_v - r_1)$, above the wing surface,

Λ is the wing sweep angle, and e_o is a surface-induction effectiveness parameter, as discussed in Section 3.5 in this Volume. (Refer to the Nomenclature Section for quantities in the text but not redefined here.)

For starting conditions in the wing root region it is necessary to estimate the value of equivalent vortex radius, r_1, corresponding to the initial two-dimension circulation strength, K_{v_e}. The data in Figure 11 of Volume I shows that, past the underexpanded jet length, x_s (determined as Y_n from Figure 13, Volume I) the spanwise jet decays much the same as a fully expanded jet, for the same pressure ratio, P_E/P_{am}. If the initial axial coordinate for the jet, ξ_i, is defined in terms of wing coordinates as in Figure A.1, then,

$$\xi_i = x_i/x_m \cos(\Lambda + \theta_o) - x_s/x_m \qquad (A.2)$$

where x_m is the wing semi-span length ($\simeq b/2$). For consistence with the terminology of Reference 16, the jet "set-back" factor, $a \simeq 0.8$, for a virtual origin is assumed to apply. Also, the cross-flow velocity ratio, redefined as $R = V_J/V_e$, is used to obtain a best-fitted relationship for the jet spreading factor $K_J(R)$ from test data in Reference 16 as

$$K_J(R) = \frac{1}{3} + 4/R \qquad (A.3)$$

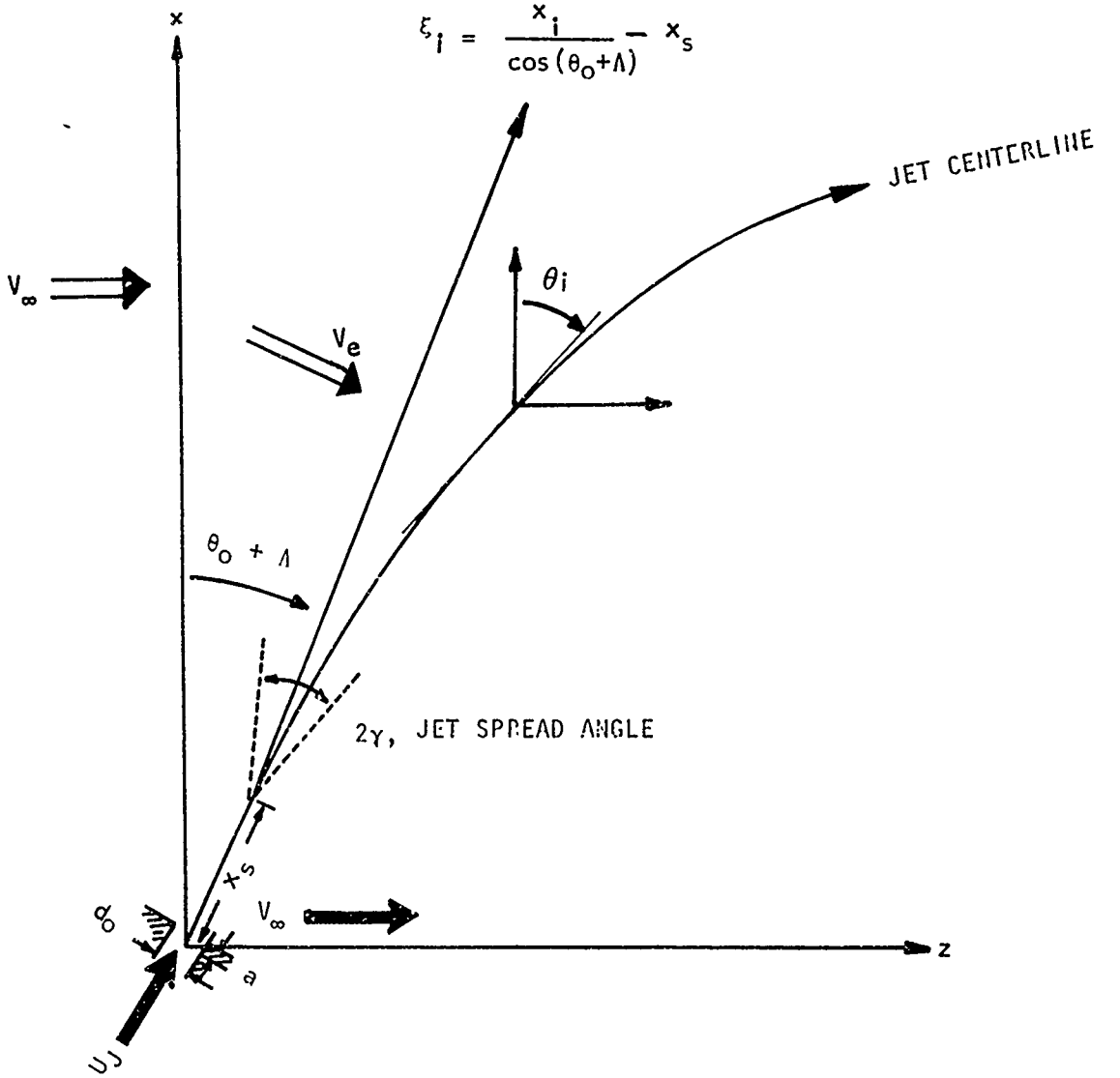

FIG. A.1 COORDINATE SYSTEM FOR JET CROSSFLOWING TRAJECTORY

ThenMcAllister's equation for jet wake depth can be written as,

$$h_i \simeq (2aD_o + A_o \xi_1 x_m) K_J(R) \qquad (A.4)$$

This is modified in two ways. D_o is the effective jet diameter at the beginning of the fully expanded region given by

$$D_o \simeq (\rho_E / \rho_{am})^{\frac{1}{2}} d_o \qquad (A.5)$$

where d_o is the true orifice diameter with ρ_E and ρ_{am} as the jet exit and ambient fluid densities, respectively. Also, A_o is an empirical growth coefficient for a wall jet which reattaches over a curved surface. From the LDV measurements (Volume I), and some data in Reference 17, $A_o \simeq 0.04$ is a reasonable estimate for present purposes. Since the jet depth tends to size the leading-edge "cavity" region, a first approximation is

$$r_i \simeq h_i/2 \qquad (A.6)$$

for $\xi_i > 1$,

so that,
$$r_1 \simeq aD_o \qquad (A.7)$$

This is not critical, since the r_i are recalculated more accurately later.

A good curve-fit of data on jet trajectories in Reference 16 can be obtained by the expressions,

$$z_i = z_J + x_s \sin(\theta_o + \Lambda) + \pi x_m \left[1 - \cos^{1/2}\left(\frac{\pi}{4} \xi_i\right)\right] + x_i \tan(\theta_o + \Lambda) \qquad (A.8)$$

and

$$\theta_i = \text{Arctan}(dz_i/dx_i) \qquad (A.9)$$

where

z_i is the streamwise deflection of the jet relative to the nozzle exit at distance z_J from the wing origin, at wing station i

and

θ_i is the jet turning angle at the same station i.

Similar adjustment of the expression (Ref. 16) for the local maximum jet velocity, U_{m_i}, results in

$$\frac{U_{m_i} - V_e}{U_J - V_e} = \frac{D\xi_s}{\xi_i + D\xi_s} \tag{A.10}$$

where $D = \mathcal{O}(1)$ (A.11)

for the cases studied.

The axially propagating velocity profile, as derived by Görtler (Ref. 37) for a free jet, is assumed to be appropriate, since it is based on the hypothesis that the eddy viscosity ν_T is constant along a cross-section of the flow, and this is consistent with initial assumptions on viscous effects in vortex flows. The equation is of the form:

$$\frac{U_{v_{ni}}}{U_{m_i} - V_e} \simeq \operatorname{sech}^2\left[A_2\left(\frac{z_{v_{ni}} - z_{J_i}}{\xi_i x_m}\right)\right] \tag{A.12}$$

for $\xi_i > 0$

where the argument for the sech is modified to include the additional jet spreading, while turning over a surface, observed in flow visualization tests (Volume I). $A_2 \simeq \pi/2$ appears to be a good approximation for these cases.

Additional equations are adopted (Ref. 16) with minor modifications. The volumetric mass flux, Q_i, is

$$\frac{Q_i}{Q_o} \simeq 1 + \left(\frac{U_J}{V_e} \cos \theta_o\right)\left(\tan\theta_i - \tan \theta_o\right) + \frac{\xi_i x_m}{B\, D_o} \tag{A.13}$$

where

$$B \simeq 9 - \left[8 \Big/ (R/9 + 1)\right] \tag{A.14}$$

and

$$Q_o = \frac{\pi}{4} d_o^2 U_J \tag{A.15}$$

The momentum flux J_i is approximated as

$$\frac{J_i}{J_o} \simeq \frac{\cos \theta_o}{\cos \theta_i} - 10\, C_f \ln\left(\frac{\xi_i + \xi_o}{\xi_s}\right) \tag{A.16}$$

where

$$J_o \simeq \rho_J U_J Q_o \tag{A.17}$$

and the last term in equation (A.16) is based on a similar expression by Newman (Ref. 17) to account for a finite friction coefficient, C_f, for a wall jet. Equation (A.17), in particular, can be improved upon by using the gas laws for compressible flow; but these expressions were found to be useful for first estimates.

For vortex dissipation effects, an initial estimate of axial flow velocity, $V_{x_{vi}}$, in outer-core regions, is approximated as follows:

$$V_{x_{vi}} \simeq U_{v_{1i}} \cos \theta_o - V_{e_1} \sin \theta_o \tag{A.18}$$

Note that, from this, a leading-edge vortex trajectory angle θ_{v1} can be estimated,

$$\theta_{v1} \simeq \Lambda + \theta_o - \gamma\left(\frac{z_J - z_{1i}}{z_J}\right) + \tan^{-1}\left[V_{ei} \cos(\Lambda + \theta_o) / V_{x_{vi}}\right] \quad (A.19)$$

Using Equation (22) of Section 3.5 in Volume II, a first order correction to the vortex augmented strength, K_{vi}, is calculated as,

$$K_{vi} \simeq \left\{ V_{\theta_{1i}} \Big/ \left[K_{ve} / (r_1 + \delta_J) \right] \right\} K_{v_e} \quad (A.20)$$

Then Owen's (Ref. 14) aging parameter, $\Lambda_i(t)$, can be approximated (in the range of interest) by the expression,

$$\Lambda_1(t) \approx \frac{1}{2} \log_{10} (10\ t_i/\tau) \quad (A.21)$$

where

$$t_i \cong \sum_{k=1}^{k=i} \left[\frac{(x_k - x_{(k-1)})}{V_{x_{v_k}} \cos(\Lambda + \theta_{v_i})} \right] \quad (A.22)$$

and

$$\tau = \frac{1}{2} r_1 (r_1 + \delta_J)/K_{v1} \quad (A.23)$$

The width of the turbulent mixing or entrainment region δ_i as sketched in Figure (A.2) presents a complex problem. The turbulence in this rate-of-strain environment must increase as the product of circumferential velocity V_{θ_i} and r_i increases, according to Rayleigh's stability criterion (Ref. 38), thus causing the radius and the mixing region to grow outward into the more stable region where the product $V_{\theta_i} \cdot r_i$ tends to decrease. To avoid an "eddy viscosity" which is variable with scale (radius of curvature), Owen (Ref. 14) defines

$$\sigma_i = \delta_i / r_i \quad (A.24)$$

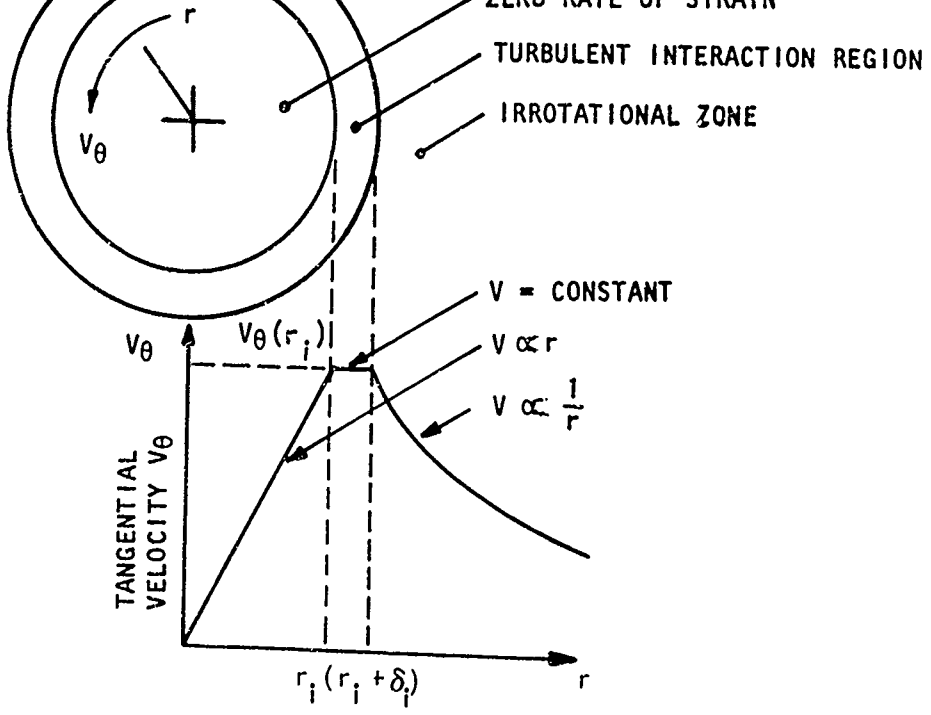

FIGURE A-2 VORTEX DECAY MODEL (REF. 14)

and

$$\lambda_i = \ell_i / r_i \qquad (A.25)$$

where ℓ is the local average, mixing length which varies along the vortex axis. The primary vortex strength (Equation A.20) is augmented by the spreading jet front as it advances, the net effect of which can be simulated as described in Section 3.5 with the vortex lattice program. However, simultaneously the turbulence develops a Reynolds shearing stress which modifies the mean (irrotational) motion, generating vorticity and allowing the extraction of kinetic energy. If the relation (Ref. 14) between the rate of dissipation and the turbulent velocity q, is accepted as:

$$\frac{d\overline{q^2}}{dt} = \frac{-\kappa\left(\overline{q^2}\right)^{3/2}}{\ell} \qquad (A.26)$$

where κ is a proportionality constant of order unity, integration of the equation for the rate of change of turbulent energy with respect to r results in an expression for the turbulent energy balance at section i as given in Reference 14. Subsequently, it is shown that for

$$\frac{\nu_{T_i}}{\nu} = \frac{1}{\sigma_i^2}\,, \qquad (A.27)$$

The corrected inner core radius r_{ci} (=r_i in Figure A.2) is given as

$$r_{c_i} = 2\sqrt{\nu_{T_i}}\sqrt{t_i} \qquad (A.28)$$

and

$$\delta_i = \sigma_i\, r_{c_i} \qquad (A.29)$$

Then the circulation strength, corrected for vortex aging, is approximately,

$$\bar{K}_{ni} \approx r_{c_i} K_{v_i}^{3/4} \Big/ \pi \nu^{\frac{1}{4}} t_i^{\frac{1}{2}} \Lambda_i(t_i) \qquad (A.30)$$

For an efficient spanwise blowing case, the vortex radial growth is quickly stabilized. For turbulence possessing an unobtrusive radial component of velocity, Professor Owen hypothesizes that $\kappa \simeq 1/\sqrt{2}$, and $\lambda \approx 5$. Since

$$\ell_i = \lambda_i \, r_{c_1} \qquad (A.31)$$

then, the scale of turbulence is about, $\ell_i \simeq 5 \, r_{c_1}$, indicating that the turbulent eddies may be predominantly axial in character in the mixing region. This seems reasonable in view of the high axial shear flow created in outer vortex layers by the coaxial jet in the case of spanwise blowing.

The point source-sink representation for velocity components is of standard form, taken directly from Reference 39, so further elaboration here is unnecessary.

Stability Criteria

Numerous vortex burst hypotheses or criteria have been studied, since it was anticipated that such instabilities would have a significant effect on the predicted vortex lift augmentation. The most consistent criterion was found to be the Rossby number, or the ratio of linear (inflow)-to-angular momentum in the vortex (References 1, 34 and 40). Reference 34 gives a particularly good discussion of this parameter (more generally used in meteorological studies); and, for a great variety of flow conditions the critical level is shown to be,

$$R_o = 0.261 \tag{A.32}$$

where a distinct change in the viscid/inviscid character of the flow occurs. This R_o magnitude is quite well verified by experiments in References 34 and 40.

Although for complex flow situations the mathematical expression is subject to interpretation, for present purposes the Rossby number is calculated as a function of position, i, along the vortex axis as follows:

$$R_{o_i} = \frac{(Q_i - Q_o)\ell_i}{2\pi r_{c_i} x_i \bar{K}_{ni}} \tag{A.33}$$

This was found to be quite successful in predicting vortex burst as observed in the test data, as discussed in Sections 3.5 and 4.2 of this Volume.

Another criterion, by Lambourne and Bryer (Ref. 41), tended to predict burst at a similar wing station using the formula

$$\left(\frac{V_{\theta_i}}{V_{x_{v_i}}}\right)^2 \left| \frac{V_{x_{v_i}} - V_{x_{v(i+1)}}}{V_{x_{v_i}}} \right| > \frac{1}{2} \quad \text{absolute} \tag{A.34}$$

Unfortunately, multiple bursts were sometimes predicted, at unlikely wing stations. The problem may arise from the difficulty in selecting the proper "stream-tube" radius, by this concept, for calculating V_θ. Also, many criteria are based on criticality concepts applicable to other than burst conditions, as discussed aptly by Hall (Ref. 42).

Some scale-effects were predicted using the Radial (inflow) Reynolds Number, as

$$R_{N_i} = \frac{Q_i - Q_o}{2\pi\nu x_i} \quad . \tag{A.35}$$

R_N is defined as negative for inflow.

Finally, the vortex Reynolds Number is given by

$$R_v = \Gamma_v/\nu \quad . \tag{A.36}$$

APPENDIX B: Background Analysis for Wake Vortex Stabilization Concept

Reference 1 presents a theoretical, viscous analysis of the Navier-Stokes equations for an axisymmetric vortex forming in a near-wake or separated flow region. By means of a transformation of the equations and a vortex-growth similarity concept, nonlinear solutions are found in terms of vortex stability modes. In particular, the Strounal frequency, S, is derived in a closed analytical form as follows:

$$S = \frac{2V_e \Omega_t r_o}{\pi V_\infty r_c} \ell n\left(\frac{r_c}{r_o\sqrt{\epsilon}}\right) \tag{B.1}$$

Where, for purposes herein, we estimate the characteristic radial dimension, r_o, is related to the wake width (Refs. 6 and 43) approximately by,

$$r_o \approx \frac{\bar{c}}{2} \sin\alpha \tag{B.2}$$

$$\Omega_t = \frac{1}{2}\left[\frac{R_N \gamma_o}{2}\right]^{1/6} \tag{B.3}$$

and

$$\epsilon = \Theta\left(8R_o^2/R_N\right) \tag{B.4}$$

For vortex shedding in the wake of a cylinder, the boundary conditions, along with the Von Karman spacing-ratio (0.281), enable determination of $V_e \cong .77\ V_\infty$, and the axial growth proportionality, $\gamma_o \cong .36$, as shown in Reference 1. The variable-separable form of solution obtained has recently been verified, during the growth period (prior to vortex breakdown), at least partially by the analysis in Reference 13.

Use of a Cauchy stretching transformation in the independent variable, r(t), jointly with a transformed stream-function $P(\psi,r)$ of mixed character in the original dependent and independent variables, results in the equation

$$\frac{d^6P}{dr^6} - \frac{R_N\gamma_o}{2}\left[P + a_1P^2 + a_2P^3 + \ldots\right] = \frac{R_N\gamma_o}{2} + f(t) \quad . \qquad (B.5)$$

For radial inflow (see Appendix A), which is characteristic of a growing wake vortex, R_N is negative. Thus, the linearized form of Equation (B.5), dropping all but the first term in brackets, results in eigenvalues corresponding to spatially periodic form for particular roots of Ω_t in Equation (B.3). With the hypothesis of characteristic vortex modes (dipole, quadropole, etc.), the Reference 1 analysis reduces Equation (B.1) to a form for S purely as a function of Reynolds Number which agrees quite well with test data for vortex shedding behind cylindrical bodies.

Because of the nature of the transformations made in Reference 1, the solution is primarily valid in outer vortical layers, or for radii beyond the hard core. It is in this outer region where the discussion in Section 3.2 of this Volume hypothesizes that R_N may effectively correspond to outflow, $R_N>0$. In that case, no oscillatory eigenvalues exist for Equation (B.5), and characteristic solutions will tend to grow without bounds. Conceptually, then, this could amount to a necessary, but perhaps not sufficient, condition for vortex burst to occur.